Lappeenranta University of Technology
Faculty of Technology
Degree Programme in Energy Technology

Lauri Halla-aho

Development of an HTR-10 model in the Serpent reactor physics code

Examiners: Dr. Tech. Riitta Kyrki-Rajamäki
M.Sc. Tech. Ville Rintala
Supervisor: M.Sc. Tech. Ville Rintala

Tiivistelmä

Lappeenrannan teknillinen yliopisto
Teknillinen tiedekunta
Energiatekniikan koulutusohjelma

Lauri Halla-aho

HTR-10 -mallin kehittäminen Serpent-reaktorifysiikkakoodissa

Diplomityö
2014
69 sivua, 23 kuvaa ja 9 taulukkoa.

Tarkastajat: TkT Riitta Kyrki-Rajamäki
DI Ville Rintala
Ohjaaja: DI Ville Rintala

Hakusanat: HTR-10, Serpent, Monte Carlo, korkealämpötilareaktori, kuulakekoreaktori

Kuulakekoreaktorimallinnuksen kuulien ja polttoainepartikkelien tarkkojen koordinaattien käyton mahdollistuminen Monte Carlo -reaktorifysiikkalaskuissa on yksi tärkeä kehitysaskel. Tämä mahdollistaa kuulakekoreaktorien tarkan mallinnuksen realistisilla kuulakeoilla ilman kuulien sijoittamista säännöllisiin hiloihin. Tässä työssä lasketaan HTR-10-kuulakekoreaktorin kasvutekijä Serpent-reaktorifysiikkakoodilla ja saadun kasvutekijän avulla reaktorin kriittiseen lataukseen tarvittava kuulamäärä. Kasvutekijä lasketaan diskreettielementtimenetelmällä tuotettuja kuulakekoja käyttäen ja kolmella eri materiaalikirjastolla tulosten vertailua varten. Saadut tulokset ovat koereaktorilla mitattua pienempiä ja jonkin verran pienempiä kuin aiemmissa tutkimuksissa muilla koodeilla saadut tulokset.

Abstract

Lappeenranta University of Technology
Faculty of Technology
Degree Programme in Energy Technology

Lauri Halla-aho

Development of an HTR-10 model in the Serpent reactor physics code

Master's Thesis
2014
69 pages, 23 figures and 9 tables.

Examiners: Dr. Tech. Riitta Kyrki-Rajamäki
M.Sc. Tech. Ville Rintala
Supervisor: M.Sc. Tech. Ville Rintala

Keywords: HTR-10, Serpent, Monte Carlo, high temperature reactor, pebble bed reactor

The use of exact coordinates of pebbles and fuel particles of pebble bed reactor modelling becoming possible in Monte Carlo reactor physics calculations is an important development step. This allows exact modelling of pebble bed reactors with realistic pebble beds without the placing of pebbles in regular lattices. In this study the multiplication coefficient of the HTR-10 pebble bed reactor is calculated with the Serpent reactor physics code and, using this multiplication coefficient, the amount of pebbles required for the critical load of the reactor. The multiplication coefficient is calculated using pebble beds produced with the discrete element method and three different material libraries in order to compare the results. The received results are lower than those from measured at the experimental reactor and somewhat lower than those gained with other codes in earlier studies.

Contents

List of figures

List of tables

List of symbols

Latin

A	area	cm^2
d	distance	cm
d	distance between parallel lines	cm
E, e	energy	MeV
F	cumulative distribution function	–
f	fraction of absorptions occurring in fuel	–
f	probability density function	–
h	height	cm
$\overrightarrow{J}$	neutron current	$\frac{1}{/}\,\mathrm{cm}^2\mathrm{s}$
k	multiplication factor	–
l	length	cm
$\hat{N}$	surface normal unit vector	–
N	amount	–
n	number density	$1/\mathrm{cm}^3$
${}^1_0n$	neutron	–
P	fraction of fast neutrons that avoid leaking	–
p	fraction of neutrons that reach thermal energies	–
Q	fraction of thermal neutrons that avoid leaking	–
q'''	power density	W/cm^3
R	reaction rate	$1/\mathrm{cm}^3\mathrm{s}$
r	radius	cm
S	surface area	cm^2
t	time	s
v	velocity	cm/s
X, Y	daughter nuclei	–
x	displacement along the x-axis	cm

Greek

β	portion of delayed neutrons	–
β^-	beta-decay	–
ϵ	ratio of total neutrons released to neutrons released from prompt fission	–
η	number of neutrons released from fission per absorption	–
ν	average number of neutrons released per fission	–
ξ	uniformly distributed variable	–
$\bar{\nu}$	antineutrino	–
ρ	reactivity	pcm
Σ	macroscopic cross section	1/cm
σ	microscopic cross section	cm^2
Φ	average neutron flux	$1/cm^2s$
φ	angle	–
$\hat{\mathbf{\Omega}}$	direction unit vector	–
$\overrightarrow{\boldsymbol{\Omega}}$	direction vector	–

Subindices

0	rounding
c	cross-sectional
cross	crossed (a line)
f	fission
m	majorant
p	reaction index
q	isotope index
s	scattering
t, total	total

List of abbreviations

ACE	A Compact ENDF
AVR	Arbeitsgemeinschaft Versuchsreaktor
BCC	Body-Centred Cubic
BWR	Boiling Water Reactor
CANDU	Canadian Deuterium Uranium
CCS	Carbon Capture and Storage
DEM	Discrete Element Method
DID	Defense in Depth
ENDF	Evaluated Nuclear Data File
FBR	Fast Breeder Reactor
FSV	Fort St. Vrain
GCR	Gas-Cooled Reactor
HTR	High Temperature Reactor
IPCC	Intergovernmental Panel on Climate Change
iPyC	Inner Pyrolytic Carbon
JEF	Joint European File
JENDL	Japanese Evaluated Nuclear Data Library
KLAK	Kleine Aufsauger Kugeln
LWGR	Light Water Graphite Reactor
LWR	Light Water Reactor
oPyC	Outer Pyrolytic Carbon
PBR	Pebble Bed Reactor
PHWR	Pressurised Heavy Water Reactor
PWR	Pressurised Water Reactor
SC	Simple Cubic
SiC	Silicon Carbide
THTR	Thorium High Temperature Reactor
TRISO	Tristructural Isotropic
UC	Uranium-Carbide

Foreword

I want to thank the Academy of Finland for making this study possible. Their funding allowed me to write a thesis about a subject I'm deeply interested in, reactor physics.

I would also like to thank my supervisor and examiner M.Sc. Tech. Ville Rintala for the guidance received during my studies, both with my Bachelor's thesis and now with the Master's thesis, as well as my second examiner Dr. Tech. Riitta Kyrki-Rajamäki for all the helpful feedback and education throughout the years.

Additionally, I want to thank my parents and grandparents for the support and push prior to and throughout my studies that helped me focus on them as a priority. I also want to give my regards to Ulrike, who has been a big support during the past year and a half.

Finally, I want to thank my old neighbour Mika Pikkarainen, who made it possible for me to start the studies at the Lappeenranta University of Technology, after my entrance examination application was lost in the post, by making sure I was able to take part in the examination.

Lappeenranta, 10.12.2014

Lauri Halla-aho

Chapter 1

Introduction

Nuclear power provides over 11 % of the electricity consumed worldwide. It is a stable power source with inexpensive fuel and virtually no CO_2 emissions [18]. Lowering emissions is increasingly important as the effort to slow down climate change is emphasized. In a report published by the Intergovernmental Panel on Climate Change (IPCC), the aim is to stop the consumption of fossil fuels without carbon capture and storage (CCS) by 2100 [8, p. 51]. In order to achieve this aim, development of renewable energy and nuclear power will be crucial in the coming decades.

Nuclear reactors being designed and under development are modelled using reactor physics codes based on deterministic and Monte Carlo methods. Codes based on Monte Carlo are a potent tool as the processing power of computers improve. At the same time more potent reactor physics codes are developed that are able to model what has been previously limited due to code restraints. An example of such a code is Serpent [17], which is able to use explicit coordinates for exact geometries in the modelling of pebble bed reactors, whereas the past codes have relied on regular lattices.

In this thesis the capability of Serpent for explicit modelling is used to model the Chinese HTR-10 reactor [5]. The point of criticality received using three different nuclear data libraries is then compared to prior studies done on the reactor. Explicitly packed pebble beds created by Heikki Suikkanen [16] are used to accurately model the core with a realistically packed bed without the use of lattices.

First the phenomena behind the function of reactors are described, followed by a description of the methods and codes used in reactor physics calculation. Finally, a description about the design of the HTR-10 and its model are given, followed by a discussion about its application.

Chapter 2

Nuclear reactors

The function of nuclear reactors requires knowledge about the behaviour of reactors from the microscopic nuclear level to the macroscopic core-wide phenomena. In this chapter the basics of the function of reactors are explained.

First, on the microscopic level, the nuclear reactions present in a reactor are explained, followed by a description of the interaction probabilities of these reactions. Then, for the macroscopic level, the basics of chain reactions, reactor control and its safety are explained. Finally a short description of the types of operational nuclear power plants is given.

2.1 Nuclear reactions

The operation of a nuclear reaction is based on a number of nuclear reactions. The major types of reaction affecting a reactor are nuclear fission, scattering and capture. These reactions together sustain the chain reaction inside a reactor and are described below.

2.1.1 Fission

Nuclear fission is one form of absorption and is responsible for producing energy and new neutrons for the chain reaction. In a fission reaction a fissile nucleus absorbs a neutron. This absorbed neutron is thermal, that is its kinetic energy is around 0.025 eV, in thermal reactors such as light water reactors (LWR).

The nuclei of atoms are held together with the strong nuclear force that counteracts the repulsive effects of Coulomb forces. As the size of the nucleus increases, the magnitude of the Coulomb force increases proportionally to the square of the total charge. Additionally, with heavier nuclei the neutron-to-proton ratio grows closer to 1.5 as opposed to 1.0 with light nuclei for the nuclei to remain stable [14, p. 9].

A low average binding energy per nucleon and an unstable neutron-to-proton ratio can make it desirable for the nucleus to split into two smaller nuclei. This would lead to a release of energy and neutrons. As an example uranium 235 releases approximately 200 MeV and 2.4 neutrons that have an average energy of 2 MeV. Such a reaction is shown in figure 2.1.

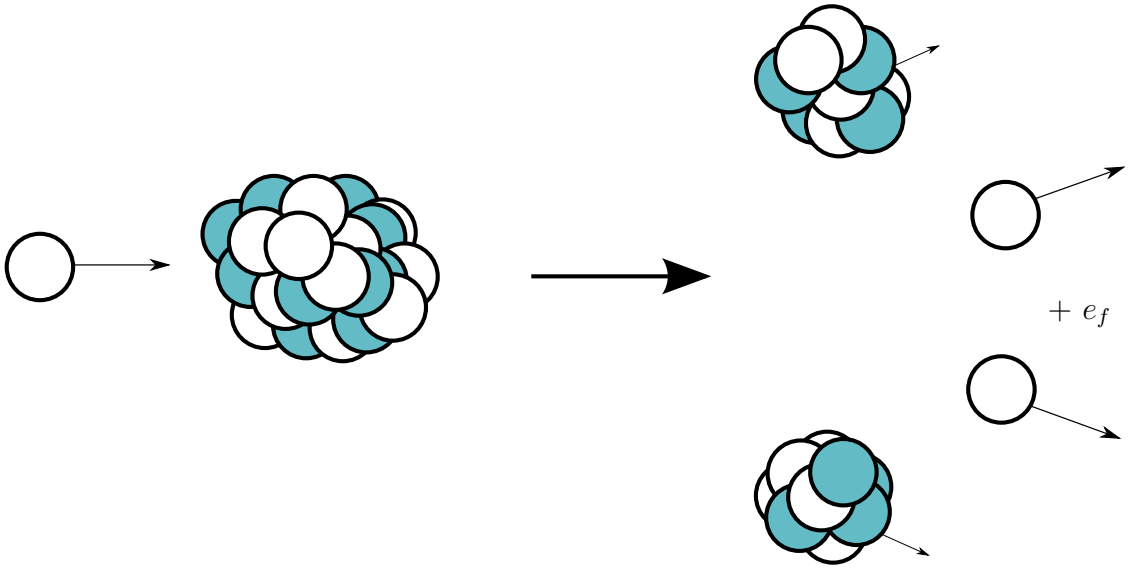

Figure 2.1: An illustration of a fission reaction.

In a reactor these neutrons are then scattered from other nuclei, absorbed or they leak out of the reactor. The energy released with the antineutrino is lost due to their weak interactions with matter. The fission of uranium-235 is depicted in the following equation:

$$ {}^{1}_{0}\mathrm{n} + {}^{235}_{92}\mathrm{U} \rightarrow \mathrm{X} + \mathrm{Y} + \nu\, {}^{1}_{0}\mathrm{n} + e_f, \tag{2.1} $$

where X and Y are the fission products, ν the number of neutrons released in the fission and e_f the energy released in the fission. The nuclei resulting from a fission reaction, called fission products, are commonly radioactive and continue decaying into new daughter nuclei mostly through β-decay.

Two most common elements viable for use as a fission fuel are thorium and uranium. Some of the main isotopes of these elements include thorium-232, uranium-235 and uranium-238. Out of these uranium-235 and -238 are the fuels of choice in conventional nuclear reactors. Uranium-235 is the source of the majority of the power of LWRs, though uranium-238 contributes through fertile capture, producing fissile plutonium-239. Thorium-232 is not fissile by itself but is fertile and thus can be made fissile through neutron capture. Due to its abundance, thorium reactors are a subject of research and development. [20]

2.1.2 Capture

In a capture reaction a nucleus absorbs a neutron but this absorption does not lead to a fission. This results in a nucleus that can undergo fission in the future if the target nucleus was fertile. The nucleus resulting from the capture is then called a fissile nucleus. Otherwise the resulting nucleus will be an isotope of the parent nucleus. [14, p. 332]

A capture reaction reduces the amount of neutrons available for fission and thus the multiplication factor but can be used to produce new fuel from fertile materials during the operation of a reactor, increasing the time before refuelling.

Such fertile materials include uranium-238 and the aforementioned thorium-232. Uranium-238 can be used to produce plutonium-239 through neutron capture. After capturing a neutron, the uranium-239 beta-decays (β^-) into neptunium-239, which further β^--decays into plutonium-239. In the thorium cycle the thorium-233 formed β^--decays into protactinium-233 which again β^--decays into uranium-233. [14, p. 318–320]

Capture reactions are also used to control the neutron flux inside a reactor and keep the reactor critical or significantly subcritical if the reactor has to be shut down. Commonly used materials include boron and cadmium. [14, p. 13]

Additionally, the neutrons can also be captured by the support structures and moderator. The irradiated structures are slowly corroded by this and become activated. Some moderators, as mentioned, are also able to capture neutrons and lose their effectiveness as a moderator. One such example is water, where the hydrogen nuclei can capture neutrons to form deuterium. As can be seen from the table 2.1 later in this chapter, the effectiveness of the nucleus as a moderator is reduced after a capture.

2.1.3 Scattering

Moderation of neutrons in a reactor is done through scattering reactions. Neutrons move through the reactor and bounce off of nuclei and slow down in the process. The two mechanisms of scattering observed are elastic and inelastic scattering. Elastic scattering requires the kinetic energy to be conserved, whereas in inelastic scattering some of the energy is transformed into the excitation energy of the target nucleus. [14, p. 200]

In elastic scattering the neutron can be scattered from the potential field of a nucleus, thus not making contact with it; or absorbed into a nucleus, which ejects a new neutron and is left in its initial state. [14, p. 200]

Elastic scattering is the main mechanism through which neutrons are slowed down in a nuclear reactor. Neutrons are scattered from the moderator, slowing down during each interaction. In thermal reactors the neutrons are slowed down to a thermal level and the average numbers of collisions required to reach this level with some moderators are listed in table 2.1. [14, p. 206]

Table 2.1: A comparison of the required numbers of collisions to reach thermal energies for commonly used moderators. [14]

Nucleus	Mass number	Collisions
H	1	15
D	2	20
C	12	92

2.2 Interaction probability

The probabilities of neutrons interacting with nuclei depend on the magnitudes of the respective cross-sections of the different nuclear reactions. The two different cross-sections used in calculations are the microscopic cross-sections σ specific to each isotope, that can be roughly said to measure the size of the nucleus and thus how high the probability of hitting it is; and the macroscopic cross-sections Σ calculated from these, which determine the probability of interaction per unit length. [14, p. 48–50]

The following derivation of the macroscopic cross section is straightforward and can be found in various seminal works in the field of nuclear engineering. Assume a space with target nuclei at which projectile nuclei are released. Each of these target nuclei is assumed spherical with a diametrical cross section σ. This is, effectively, the projection of the target nuclei on a plane perpendicular to the direction of the projectile nuclei. An illustration of this is shown in figure 2.2.

The macroscopic cross section Σ is a constant used to express the probability of a collision occurring over a distance. The probability of such an event occurring within dx after a neutron has travelled a distance x without collisions is defined to be Σdx. Consider a cuboid section of the aforementioned space with a surface area of S on the faces perpendicular to the direction of the projectiles and a height of dx. In this section there are N target nuclei, the projections of which do not overlap. The nuclei then effectively occupy a volume of $N\sigma dx$.

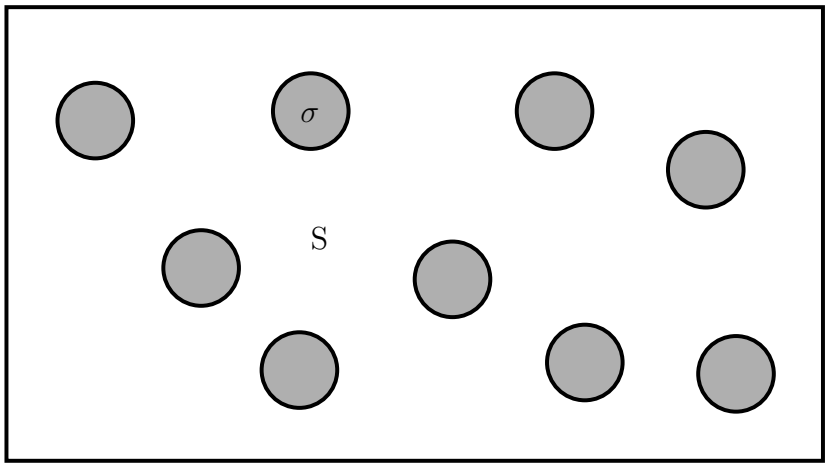

Figure 2.2: 2D projections of non-overlapping spherical targets.

The probability of hitting a target nucleus is then the ratio of the above volume and the total volume of the cuboid, Sdx. However, since the probability of a collision occurring within this section of space has been defined to be Σdx, the macroscopic cross section can be written as:

$$\Sigma = \frac{N\sigma}{Sdx} = n\sigma, \tag{2.2}$$

where n is the number density of neutrons [1/cm^3], the number of neutrons per unit volume. The microscopic cross-sections are generally inversely proportional to the ve-

locity of the neutron v, that is $\sigma \propto 1/v$. However, between the fast and thermal energies the neutrons are susceptible to resonance captures, which behave more erratically. [14, p. 54]

In the resonance part of the energy spectrum the sum of the binding energy of a neutron and its kinetic energy can be equal, or close, to the energy required to bring the nucleus to an excited state. This makes it easier for a fission to occur, however the most common reaction with resonance is the neutron capture. [14, p. 57–58]

The Doppler effect or the Doppler broadening is important to consider with the absorption cross sections in the resonances of nuclei, especially uranium-238. Since the cross sections are a function of the relative velocity of a neutron to the target nucleus, changes in the speed of the target nucleus have an effect on the cross section. Thus the effect of the change depends on the rate of change of the cross section. Near a resonance peak this change can then lead to a significant change in the cross section. [14, p. 246–247]

2.3 Chain reaction

In a chain reaction the neutrons released from fission eventually cause new fission reactions, releasing more neutrons. Such a reaction can sustain itself and thus be used for energy production.

Each fission of uranium-235 caused by a thermal neutron releases on average 2.4 neutrons. This means that, if no neutrons leak out of the reactor or are captured, the amount of neutrons in the reactor is multiplied by a factor of 2.4 between each generation. A simple illustration of this is shown in figure 2.3. This does not happen, however, in reality due to the aforementioned losses of neutrons.

The six factor formula for determining the multiplication factor of a non-infinite reactor, that is the ratio of neutrons between successive generations, is:

$$k = \eta \epsilon p f P Q, \tag{2.3}$$

where k is the multiplication factor, η the number of neutrons released from fission per absorption, ϵ the ratio of total number of neutrons released from fissions to the number of neutrons released from thermal fissions, p the probability that the neutron is not absorbed before slowing down to a thermal energy, f the probability that an absorbed neutron gets absorbed in fuel, and P, Q the probabilities that a fast neutron and a

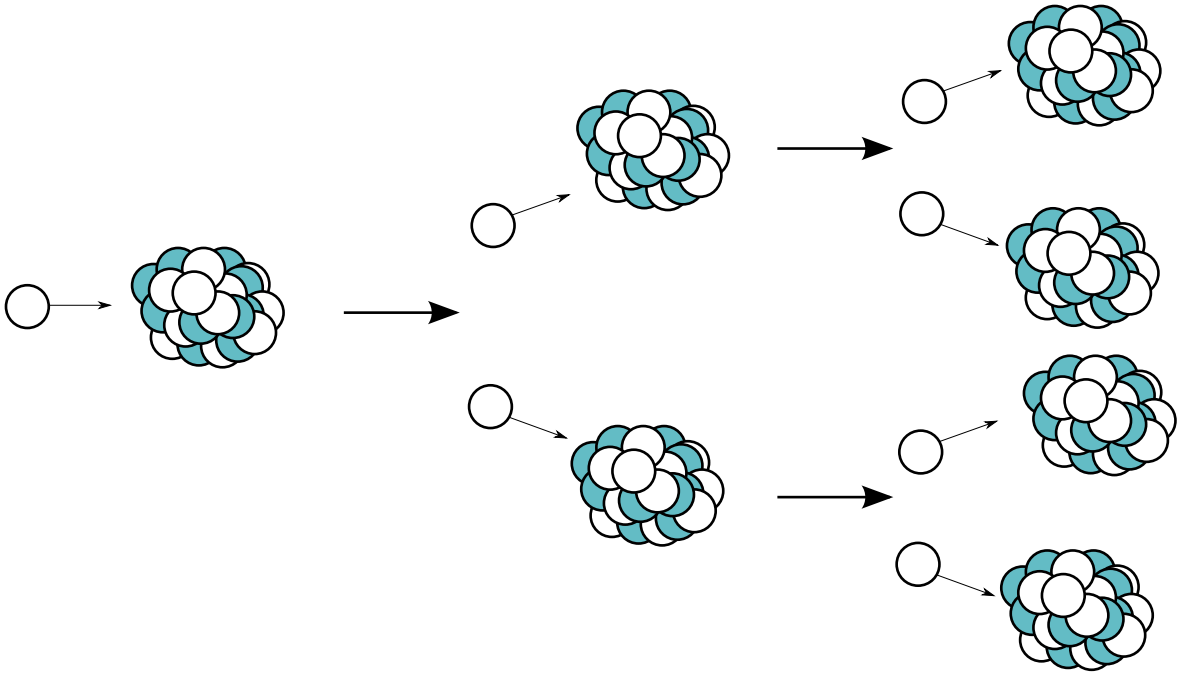

Figure 2.3: An illustration of a chain reaction.

thermal neutron does not leak out of the reactor, respectively.

Depending on the value of k the behaviour of the reactor varies significantly. If $k < 1$, the reactor is subcritical. This means the amount of neutrons present in the reactor will decrease exponentially until it reaches zero or the level determined by a neutron source if one is present. [10, p. 290]

If $k = 1$, the reactor is critical. Then the amount of neutrons released from the fissions of each generation equal to the amount of neutrons lost during that same generation. Thus the amount of neutrons stays constant unless there is a neutron source, in which case it will increase at a constant rate.

Finally, if $k > 1$, the reactor is supercritical. This causes the amount of neutrons and thus the power output to increase exponentially. A special case of this is when $k \gtrapprox 1 + \beta$, where β is the portion of delayed neutrons out of all produced neutrons.

Delayed neutrons are released a short delay after the fission. On the other hand the neutrons released immediately from fission are called prompt neutrons. When the portion of delayed neutrons is less than the supercriticality of the reactor, the reactor is in a promptly critical state. In this state the only remaining method of controlling is through Doppler broadening.

Another way of representing the criticality of a reactor is through reactivity ρ:

$$\rho = \frac{k-1}{k}. \tag{2.4}$$

The sign of ρ thus indicates the criticality of the reactor: a negative sign means it is subcritical whereas a positive sign indicates supercriticality. The reactor is critical only when the reactivity is zero.

2.4 Control

The reactor is kept at criticality during operation in order to produce a constant power output. This is affected by, for example, absorbent materials, reactivity feedback, moderation and delayed neutrons.

Absorbent materials, such as those found in control rods, reduce the reactivity by absorbing free neutrons. Safety rods are kept outside the reactor to guarantee negative reactivity in the case of a sudden positive reactivity transient. Others are continuously inserted and retracted from the reactor as the reactivity changes.

When a reactor has a negative feedback with respect to a given state variable such as temperature or void fraction, its reactivity is reduced when the value of the variable in question increases. This allows for additional ways of controlling the operation during sudden power spikes. Example phenomena include the moderator heating up and boiling, increasing the void fraction and thus reducing the moderation, which reduces the amount by which the neutrons are able to slow down; and the rise of the temperature of uranium, which causes the resonance absorption peaks to broaden and thus reduces the power output.

The existence of delayed neutrons is a significant aid in the control of a reactor. The life times of prompt neutrons are too short to be controlled through the aforementioned means but the longer effective life time of the delayed neutrons, approximately increasing the effective life time of neutrons by a factor of 1,000 due to the delay in their release, allows for the control of reactors.

2.5 Safety

One of the main concerns with nuclear reactors is their safety. Utmost care must be taken when designing the safety systems and barriers between radiation and the environment. The main goal, however, is to make the reactors inherently safety. This includes ensuring the aforementioned negative feedback in the reactor to prevent its power output from increasing when, for example, the temperature rises.

The approach of utilizing multiple layers of protection and ensuring the effectiveness of these barriers is called defense in depth (DID). The aim of DID is to remove the effects of human and component failures, prevent damage to the power plant and the barriers, and to protect the people and environment in the case the barriers fail. [7, p. 4]

The aim of DID is to prevent any possible accidents and, if this does not succeed, minimize the possible damage and harm caused and prevent the accident from becoming worse. It is traditionally split into five nested layers. Once a layer fails, the next layer attempts to mitigate the damage and prevent further problems. The five layers and their aims are listed in table 2.2. [7, p. 4–5]

Table 2.2: The layers and their aims of defense in depth. [7]

Layer	Aim	Description
1	Prevent maloperation and failures	Quality ensurance of construction and operation, conservative design
2	Control maloperations and failures	Systems for detection, control and limiting of failures as well as protection from further negative developments
3	Control accidents	Designed safety systems and measures
4	Manage severe conditions and prevent further progress of failures	Accident management
5	Minimise the effects of the fallout	Emergency procedures

Environmental phenomena such as earthquakes, floods and fires can breach multiple layers at once. As such, protection from their effects need to be included in the design of the power plant. Systems vital to the reliable operation of the plant, such as electrical centres, backup power generators and reactor control mechanisms, should be made safe from these risks. [7, p. 7]

Another important factor in the defense from radioactive releases are the physical barriers built into the fuel, reactors and building structures. These barriers vary between different types of reactors. For example, in the case of most water reactors, these layers are the cladding of the fuel, the coolant circuit and the containment building. The cladding is designed to be able to retain both solid and gaseous fission products. The containment of the coolant circuit is aimed to retain any products released from the fuel and finally the containment building of the reactor is built to hold the released radioactive material. [7, p. 8]

2.6 Reactor types

There are a number of different types of reactors differing for example by their choice of fuel, moderator and coolant. The power reactors operating globally at the end of 2013 can be split into six major groups: pressurised water reactors (PWR), boiling water reactors (BWR), pressurised heavy water reactors (PHWR), gas-cooled reactors (GCR), light water graphite reactors (LWGR) and fast breeder reactors (FBR). Their amounts, gross power outputs and fuel, moderator and coolant choices are shown in table 2.3. [19]

Table 2.3: A compilation of the amounts of operational reactors and their properties. [19]

Type	Amount	Output [GW_e]	Fuel	Moderator	Coolant
PWR	273	253	UO_2, enriched	H_2O	H_2O
BWR	81	76	UO_2, enriched	H_2O	H_2O
PHWR	48	24	UO_2, natural	D_2O	D_2O
GCR	15	8	U, natural	CO_2	graphite
			UO_2, enriched		
LWGR	15	10.2	UO_2, enriched	H_2O	graphite
FBR	2	0.6	UO_2	Na, liquid	none
			PuO_2		

PWRs and BWRs use light water as both the moderator and coolant along with enriched uranium dioxide as the fuel. PWRs have pressurised primary circuits with the water at approximately 150 times the atmospheric pressure. This is done to prevent a phase change. The secondary circuit is held at a lower pressure and the heat between these circuits is transferred through the heat exchangers and used to boil the water on

the secondary side, which is then passed through the turbines. This allows the water of the secondary loop to remain uncontaminated by the reactor. [19]

BWRs, on the other hand, rely on a single circuit where the coolant flows through the reactor, boils and is then passed through the turbine. They operate at a lower pressure, around 75 atmospheric pressures. Due to the single circuit design, during operation the turbine is contaminated by the radioactive N-16 produced. [19]

The commonest type of a PHWR is the Canadian deuterium uranium (CANDU) reactor. Its use of heavy water as the moderator and coolant allows the use of natural uranium as fuel. This increases the amount of produced nuclear waste but raises the amount of energy produced per unit mass of uranium. Additionally, the CANDU is able to be refuelled during operation through the use of pressure tubes as a containment for the fuel elements inside the coolant tank, calandria. [19]

Chapter 3

Reactor physics calculation

At a given point in space, the number density of neutrons or the number of neutrons observable within a unit volume is n [1/cm^3], as was defined in section 2.2. Assume v to be the speed of the observed neutrons. Then the probability of a neutron interacting with matter in a time dt is $\Sigma v dt$. If this is multiplied by the number density of neutrons, the number of reactions within a unit volume during dt is received. Thus the reaction rate R [1/cm^{3}s], the number of reactions within a unit volume and unit time, is: [14, p. 98]

$$R = \Sigma n v \tag{3.1}$$

The term nv appears often in nuclear engineering. It is commonly substituted with the neutron flux Φ [1/cm^{2}s]. With this substitution, the above equation can be rewritten as:

$$R = \Sigma \Phi \tag{3.2}$$

Unlike a conventional flux, the neutron flux does not measure neutrons passing through a surface but instead is a volumetric quantity [14, p. 98]. As such it is a scalar quantity and is not dependent on the direction. It can be thought of as a collection of neutrons diffusing through matter, similar to the diffusion of gas.

This, however, is not accurate due to the tendency of the neutrons to travel large distances between collisions. A more accurate method is to find the solution to the neutron transport equation [3, p. 113]:

$$\frac{\partial n}{\partial t} + v\hat{\boldsymbol{\Omega}} \cdot n + v\Sigma_{\mathrm{t}} n\left(\boldsymbol{r}, E, \hat{\boldsymbol{\Omega}}, t\right) = \int_{4\pi} d\hat{\boldsymbol{\Omega}}' \int_0^\infty dE' v' \Sigma_{\mathrm{s}}\left(E' \to E, \hat{\boldsymbol{\Omega}}' \to \hat{\boldsymbol{\Omega}}\right) n\left(\boldsymbol{r}, E', \hat{\boldsymbol{\Omega}}', t\right) + s\left(\boldsymbol{r}, E, \hat{\boldsymbol{\Omega}}, t\right), \quad (3.3)$$

where s [1/cm^{3}s] is the neutron source term and $\hat{\boldsymbol{\Omega}}$ the direction unit vector of the flux. The neutron flux is of interest in reactor physics calculations. This is because it determines many of the variables of interest. These variables include the above reaction rate R, power density q''' and burnup.

Another important quantity in neutron physics is the neutron current $\overrightarrow{J}$ [1/cm^{2}s]. Its concept is closer to that of other fluxes since it measures the number of neutrons passing through a surface. Unlike the flux, the neutron current is a vector quantity and thus its direction matters in calculations. The current is related to the flux through [14, p. 100]:

$$\overrightarrow{J}\left(\overrightarrow{\boldsymbol{\Omega}}\right) = \overrightarrow{\boldsymbol{\Omega}}\Phi\left(\overrightarrow{\boldsymbol{\Omega}}\right), \quad (3.4)$$

where $\overrightarrow{\boldsymbol{\Omega}}$ is the direction vector of the flux. A surface, through which the current flows, has a surface normal unit vector $\hat{N}$. The full angle between the direction of the flux and the normal is θ and the direction is positive if θ is between 0 and $\pi/2$ and negative when between $\pi/2$ and π. The currents against a surface, in their respective directions, can then be represented with:

$$J_+ = \int_{0<\theta<\pi/2} \overrightarrow{J}\left(\overrightarrow{\boldsymbol{\Omega}}\right) \cdot \hat{N} d^2\boldsymbol{\Omega} \quad (3.5a)$$

$$J_- = -\int_{\pi/2<\theta<\pi} \overrightarrow{J}\left(\overrightarrow{\boldsymbol{\Omega}}\right) \cdot \hat{N} d^2\boldsymbol{\Omega} \quad (3.5b)$$

One approach of solving equation (3.3) is to find a numerical solution deterministically because an analytical one is a practically impossible. This can require significant homogenisation of the materials due to the vast amount of neutron fluxes to be solved all around the reactor. Another option is to use statistical methods to track individual neutrons and thus determine the neutron fluxes throughout the reactor. One example of such a method is the Monte Carlo method.

3.1 Monte Carlo method

The historical Monte Carlo method was first used by Comte de Buffon in 1777 to approximate π by dropping needles onto a sheet with regularly distanced parallel lines. Calculating the portion of needles crossing a line, he could get an estimate with

$$\pi = \frac{2lN_{\texttt{total}}}{dN_{\texttt{cross}}}, \tag{3.6}$$

where l is the length of the needle, d the distance between the parallel lines and $N_{\texttt{total}}$, $N_{\texttt{cross}}$ the number of total needles and needles that crossed a line, respectively. [2, p. 11]

In the Monte Carlo method the desired quantities are represented by stochastic variables. These random values follow the probability distributions of the physical quantities they represent. This probability distribution is then used to determine the outcome of a reaction after a random value for the variable has been sampled.

While Monte Carlo method is effective at microscopic calculation, such as tracking individual neutrons or photons, it struggles with macroscopic calculation, such as particle fields. With complicated simulations, where the dimensions of the problem exceed 4, the Monte Carlo method is likely to converge more efficiently. [2, p. 7–8, 158]

The method is commonly used with reactor physics codes in nuclear engineering. Consider as, an example, the sampling of the distance x a neutron travels prior to colliding with a nucleus in a given medium using a delta-tracking method. If the neutron is produced from a fission occurred during a previous cycle, its energy and direction of travel are sampled first. The medium in which the neutron travels, as well as its neighbouring material regions, has a significant impact on the distance traversed. In a given medium, the probability density function of a free path for a neutron is given by [11, p. 98]:

$$f(x) = \Sigma_{\mathrm{t}} e^{-x\Sigma_{\mathrm{t}}}, \tag{3.7}$$

where $f(x)$ is the probability density function for the distance x that the neutron travels and Σ_{t} the total macroscopic cross section. Thus the cumulative distribution function $F(x)$ is, through integration [11, p. 98]:

$$F(x) = 1 - e^{-x\Sigma_{\mathrm{t}}}. \tag{3.8}$$

By marking $F(x)$ as ξ, a uniformly distributed random variable between 0 and 1, the solution for x can be written as [11, p. 98]:

$$x = -\frac{1}{\Sigma_\mathrm{t}} \ln \xi, \tag{3.9}$$

thus allowing the random sampling of free paths using pseudo-random numbers.

After the sampling of the free path, the reaction the neutron undergoes is solved. Due to the delta-tracking, the total macroscopic cross section in equation (3.9) is represented by the majorant total cross section Σ_m, that is the highest local cross section, of the material region. The majorant makes the calculation faster through the omission of the material checks. Problems may arise near highly absorbant material due to a number of virtual collisions experienced through this method and due to the lack of a capability to estimate the neutron track lengths. [11, p. 101–103]

When the point of collision is determined by sampling the free path, the virtuality of this collision has to be checked. If it is found to be a virtual collision, a new free path will be sampled using the local majorant. Otherwise the type of a reaction is sampled next. The collision is virtual if:

$$\xi \leq \frac{\Sigma_\mathrm{t}(\overrightarrow{\boldsymbol{r}})}{\Sigma_\mathrm{m}}, \tag{3.10}$$

where $\Sigma_\mathrm{t}(\overrightarrow{\boldsymbol{r}})$ is the local total macroscopic cross section at the point of collision. In the case of a collision, the type of nuclear reaction is sampled next. In this case the solution is found through the cumulative sum of the component macroscopic cross sections.

Next the nuclear reaction occurring with an isotope of the material is sampled. Given the reaction k, on an isotope i, its probability $p_{k,i}$ can be represented by the aforementioned uniformly distributed random variable ξ. This leads to the range of ξ, where the reaction k occurs on the aforementioned isotope i, to be [11, p. 103–104]:

$$\frac{\sum_{p=1}^{k-1} \sum_{q=1}^{i-1} \Sigma_{p,q}}{\Sigma_t} < \xi \leq \frac{\sum_{p=1}^{k} \sum_{q=1}^{i} \Sigma_{p,q}}{\Sigma_t} \tag{3.11}$$

If the sampled reaction is fission or neutron capture, the history of the neutron in question ends. In the case of fission, prompt and delayed emitted neutrons are sampled for the next cycle and the history of the old neutron is terminated. If the neutron

scatters, its history continues, a new direction and the energy loss are sampled and, in the case of an inelastic collision, possible additional released neutrons. The Monte Carlo method requires the sampling to be repeated a vast number of times to reduce the statistical error, which is inversely proportional to the square root of the amount of quantities sampled. [11, p. 104–106]

In reactor physics calculations, the Monte Carlo method thus follows the lives of individual neutrons from their generation to the ends of their histories. They are generated from fissions sampled during the previous generation or artificially added into the reactor to raise the amount of neutrons to a fixed number if the neutron multiplication coefficient is less than one.

The tracks of the neutrons can be determined using ray tracing or delta-tracking methods. In ray tracing the free path of the neutron is sampled and, if it exceeds the optical distance to the closest boundary between different material regions, is moved to the boundary and a new free path is sampled; otherwise it is moved to the sampled location. The delta-tracking process is described above. [11, p. 99]

The histories of the neutrons end once they are absorbed, as described before, or leak out of the reactor. In the case of an occurrence of a fission reaction, the number of neutrons released is sampled. This approach is called analog since it follows the physical process closely. A non-analog approach would be not to end the history of the neutron but to reduce its statistical weight and end the history when the weight of the neutron has become low enough. [11, p. 118, 128]

It is then possible to determine the multiplication coefficient from the ratio of the neutrons at the beginning of the generation and at its end. However, due to the slow decrease in the error of the method, it demands a lot of computation time. As previously mentioned, if the error is to be, for example, halved, the sample amount and thus the computation time must be quadrupled.

3.2 Deterministic method

Deterministic methods divide the volume into a number of nodes, cells or other smaller sections. These sections are then given an average neutron flux or a neutron flux function that approximates the shape of the neutron flux distribution in that area.

In an example reactor there can be 200 fuel assemblies, each of which contains 289 fuel rods. These rods are usually split into at least 10 radial and 50 axial sections. Around a hundred different directions are chosen for the neutrons to move in. The number of points on the energy meshes for the cross section calculations are often on the order of magnitude of 10,000. Calculating the evolution of the reactor over time also requires tens of calculations. Considering all of the above, the number of neutron flux values that have to be solved is on the order of 10^{15}. [14, p. 497]

Due to this complexity the deterministic solutions require the calculations to be divided into multiple steps. This calculation chain begins with the collection of evaluated nuclear data. This includes multiple measurements of nuclear reactions and interactions that are weighed and averaged in standardized nuclear data libraries. [14, p. 78–80]

The calculation variables, notably the cross sections, are discretised into multiple groups with regards to energy, velocity, location and direction. The amount of groups is usually on the order of a hundred. The group cross sections are homogenised in material regions, such as the fuel pin lattices or assemblies. This can be done, though to a lesser degree of accuracy, with [14, p. 506]:

$$\Sigma_M = \frac{\sum_{m \in M} V_m \Phi_m \Sigma_m}{\sum_{m \in M} V_m \Phi_m}, \tag{3.12}$$

where m is a given subzone of a larger zone M and V_m [cm^3] the volume. This homogenisation method is not able to conserve the reaction rates in the macroscopic zones. An equivalence equation that conserves the reaction rates of every reaction α in a group g is: [14, p. 506]

$$V_M \Phi_{M,g} \Sigma_{\alpha,M,g} = T_{\alpha,M,g}, \tag{3.13}$$

where T [1/s] is the reaction rate data from a reference calculation. This calculation chain then progresses from individual nuclei to the defined fuel pins, fuel assemblies and finally to full core calculations.

The nuclear data libraries are used to generate cross section group constants for the nuclides. These are then used to generate group fluxes for the rods and the process is repeated for each cell in the assembly. The fluxes can then be used to homogenise the cells with a small group count, on the order of tens instead of the earlier hundreds, though with LWRs only two energy groups are commonly used. These fluxes are then

used to generate group fluxes for the whole assembly.

The detail of the reactor thus is reduced the further the calculations progress from the nuclear level to core-wide. This prevents the calculations from becoming impossible to solve or taking a long amount of time. The gradual reduction in detail resulting from discretisation and homogenisation reduce the accuracy of the results.

3.3 Reactor physics codes

Reactor codes simulate the operation and behaviour of whole reactors. They can be used to determine the neutron flux and temperature distributions, burnup and power density among others. They can thus be used to guarantee that, for example, the power density of the reactor does not exceed the limits set by the regulations. Another applications for the reactor physics codes include finding out the circumstances in which the reactor can reach criticality, and determining the evolution of the fuel through in core fuel management.

Reactor codes can be used to solve the systems with one-, two- or three-dimensional calculation. They can be solved through deterministic or stochastic methods. Some examples of the deterministic reactor physics codes are CASMO, which performs calculation on the assembly level; ARES, which is used for full core calculations; and HEXTRAN, which is applied in transient modelling. Examples of the stochastic, here using the Monte Carlo method, reactor physics codes include MCNP, MONK, Serpent, TRIPOLI, TWOTRA and VSOP.

Out of the Monte Carlo codes MCNP is perhaps one of the most commonly used. It can be used to simulate 3D configurations, model geometry and determine reactor criticalities accurately. However, its limitations, and most of the other codes, become apparent with pebble bed reactors. It is not possible to model randomly packed pebbles in MCNP and thus pebble bed reactors have to instead have the pebbles placed in lattices, which reduces the accuracy of the simulation. This is because the pebbles are dropped in the core instead of placed in a regular lattice, causing their placement to be irregular. [5, p. 281, 283]

3.4 Serpent

Serpent is a three-dimensional Monte Carlo reactor physics code developed at the VTT Technical Research Centre of Finland and specializes in burnup calculation and group constant generation as well as LWR simulation. Serpent also incorporates additional geometry types for high temperature reactors. [17]

Serpent uses ACE-format nuclear data libraries such as JEFF-3.1.1 and ENDFB/B-VII. Their cross section data is transformed into a unionised continuous-energy grid to speed up calculations by removing extra iterations during the simulation. This comes, however, with an added cost in the required memory to store the cross section data. [17]

Serpent is able to utilize both ray tracing and delta-tracking methods in the simulation to speed up the calculations significantly. This is because the delta-tracking allows for crossing material boundaries without checking the shortest optical distances to the said boundaries. It can cause the neutron flux estimator to be inaccurate in small volumes. [17]

Additionally, it does not require the placement of pebbles or particles in lattices. Instead, Serpent is able to use randomly generated explicit coordinates for fuel particles and pebbles. This allows for a realistic representation of the fuel particle and pebble distributions. It also allows the use of separately generated, for example through the discrete element method (DEM), pebble beds.

Chapter 4

High temperature reactors

The high temperature reactors have been under development since the late 1950s. Their potential for inherent safety makes then a noteworthy option for nuclear power in the future. In this chapter their background and properties are described.

First the history of the high temperature reactors is explained, followed by descriptions of their design and modularity. Finally, the core, fuel and safety of the HTR-10 reactor are described.

4.1 History

Among the first high temperature reactors (HTR) were the Dragon in UK, Arbeitsgemeinschaft Versuchsreaktor (AVR) in Germany and Peach Bottom in USA. The Dragon experiment was started in April 1959 and reached full power by April 1966. The aim of this project was the start of the development of required technology and the demonstration of the viability of HTR technology. The reactor used graphite elements with coated uranium-carbide (UC) fuel particles. The reactor was used in the research of helium-cooled reactors and fuel particle coatings and was operated at full capacity for long periods of time . [4, p. 5]

The AVR was operational from 1967 until 1988. Its core contained graphite pebbles in a pebble bed, with the spheres having a diameter of 6 cm. It was thus used to develop the pebble bed -type reactors and to support the omission of an LWR-type containment barrier. [4, p. 5]

Following these test reactors were the Fort St. Vrain (FSV) in USA and the thorium

high temperature reactor (THTR-300) in Germany. The fuel used in FSV comprised of hexagonal fuel blocks that contained TRISO coated (tristructural isotropic) fuel particles. The reactor experienced many downtimes due to mechanical problems in the helium circulators. Nevertheless FSV was used in the demonstration of the function of multiple systems, such as steam generators and the aforementioned fuel blocks. THTR-300 was shut down early after only five years of operation due to a lack of funding. However, it was still effective in the validation of security systems and thermodynamics. [4, p. 6–7]

In the 1980s the development of modular HTRs started. First of these was a German HTR-MODUL, which started with a safety assessment in 1987. Among the major planned safety features of the reactor were the inability of the reactor to reach temperatures of 1,600 ℃, the removal of decay heat during emergencies without active cooling, possibility of a shutdown through a drop of absorber pebbles into absorber channels bored into the reflector, and the use of chemically neutral gas as a coolant. [4, p. 7–8]

The development of HTRs in China began in the 1970s. Initial plans involved breeder reactors using a thorium cycle but this was later abandoned and replaced with a uranium cycle. The research into a thorium cycle did, however, help in the development of, for example, helium technology and coated particles. [6, p. 1–2]

In the 1980s China started to cooperate with the German Jülich Nuclear Research Centre. Progress was made in the development of codes, safety and fuel and the use of moderator fuels in the centre of the core, surrounded by fuel pebbles, allowing a power output of 500 MW_e. Research was also made toward the applications of HTRs in reducing the use of fossil fuels in various industries. [6, p. 2]

In 1986 they started developing, with international cooperation, some of the critical components such as modular design, helium technology and pebble bed flow. Major progress was made in the production of the fuel particles and their coating. Following this, in 1992 the construction of a 10 MW_{th} test reactor, HTR-10, was approved. The construction started in 1995 and was finished in 2000 when the reactor was loaded and reached criticality. [6, p. 2–3]

4.1.1 The Dragon reactor

The Dragon reactor, as mentioned above, was among the first HTRs and was designed to have a thermal output of 20 MW_{th}. The reactor, shown in figure 4.1, used prismatic fuel, that is the fuel particles were located within hexagonal graphite blocks. Each fuel element had a fuelled central section along with graphite reflectors on the top and bottom. The core consisted of 37 clusters of seven fuel blocks. Surrounding these elements are the reflector blocks with holes for 24 control rods. [13, p. 62–63]

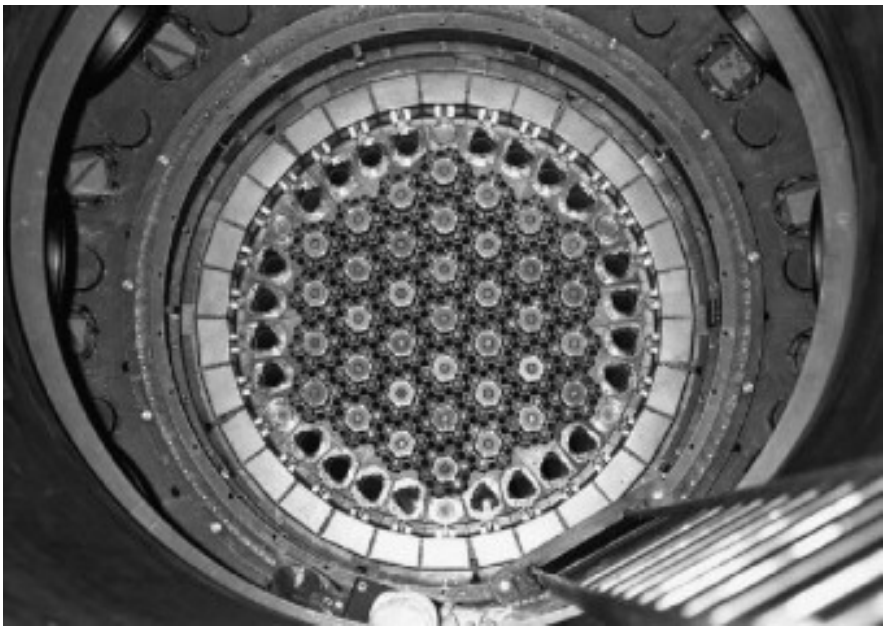

Figure 4.1: View from above on the Dragon reactor core. [13, p. 62]

The possibility of utilising a wide variety of fuels, convert fertile materials into fissile, reach high burnup and conversion ratios as well as refuelling during operation made the HTR a desirable option. This was aided by the ability of the coated fuel particles, shown in figure 4.2, to retain the fission products better than expected. This showed that the coolant purification plants were designed for a higher capacity than necessary. [13, p. 63]

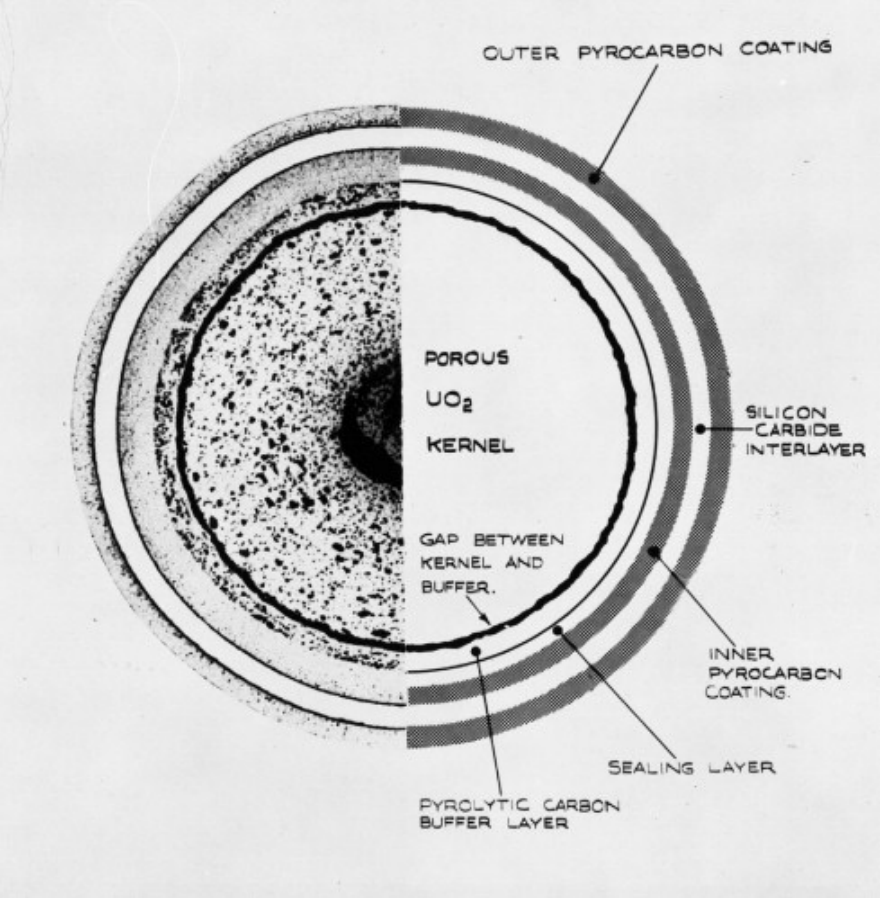

Figure 4.2: A cross section of the fuel particle used in the Dragon reactor. [13, p. 66]

Some modifications to the reactor were necessary during its lifetime. They showed that, due to the low contamination level of the primary circuit of the reactor, maintenance was easy to perform. The reactor reached criticality in 1964 with 16 inserted fuel elements. [13, p. 64]

Among the legacies of the Dragon reactor were coated fuel particles. In the search for fuel capable of holding the gaseous and volatile fission products, it was initially suggested that the fuel particles would be coated with pyrolytic carbon. It was found to be insufficient by itself and research into suitable metallic carbides able to retain such products without absorbing neutrons began. Silicon carbide and zirconium carbide were possible options and the earlier was chosen as an additional coating. [13, p. 64–65]

4.2 Design

High temperature reactors are a type of fourth generation nuclear reactors currently under research. They use graphite as a moderator, a gas or a molten salt as a coolant

and are designed to reach temperatures higher than LWRs. Two possible types of HTR reactors are prismatic graphite cores, where the fuel is placed inside hexagonal graphite blocks; and pebble bed cores, where the fuel is inserted inside graphite pebbles that are stacked inside the reactor. In this thesis the focus is on the pebble bed reactors.

The pebble bed reactor (PBR) fuel can be continuously renewed and recycled by removing used fuel from the discharge tube. Figure 4.3 shows a simplified illustration of this process. These fuel pebbles are then returned to the core if their burnout and condition allow. This allows for a high uptime of the reactor due to the lack of a need for an annual shutdown. [9, p. 334]

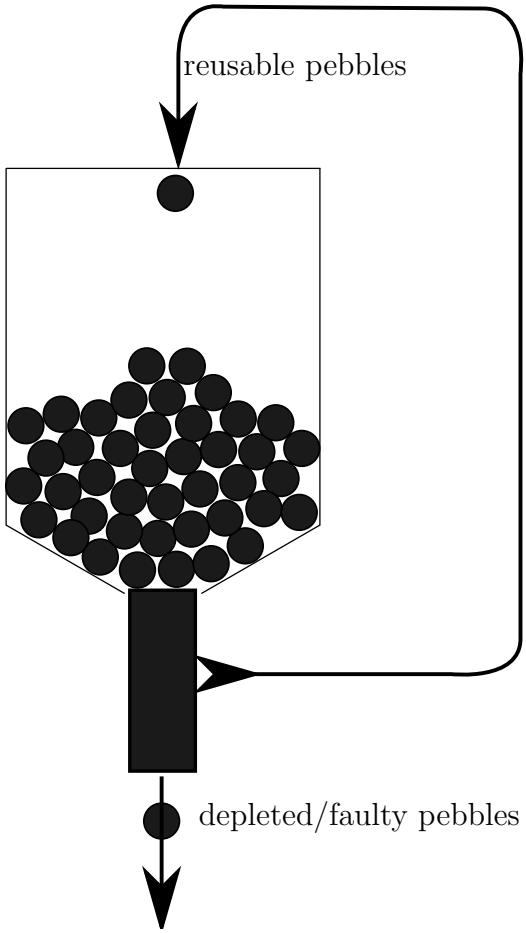

Figure 4.3: Fuel recycling in a pebble bed reactor.

An HTR can be designed to be inherently safe by making the fuel able to endure the highest achievable temperatures, during operation and due to decay heat, without cooling. The effects of Doppler broadening eventually increase enough to reduce the power output enough to stop the increase of temperature. The fuel pebbles of HTR-10 reactor, for example, can in theory withstand approximately 1,600°C without releasing any fission products. Thus an active cooling system is not required in the case of an

accident and the heat can be removed passively from the reactor core. [21, p. 25–26]

Another benefit of the HTRs over conventional LWRs is the higher thermal efficiency reachable with HTRs. Whereas the typical thermal efficiency of LWRs is around 32–36 %, the HTRs can reach a thermal efficiency of about 45 %. This reduced the amount of fuel required to produce the same amount of electricity by a significant margin. [9, p. 336]

The pebble bed reactors do, however, have some risks resulting from the choice of fuel. The fuel pebbles are prone to grind against each other and can thus release dust that can eventually become activated and accumulate on the heat exchangers of the steam generators [15, p. 1]. This reduces the power output and increases the core temperature due to the reduced amount of heat transferred.

Another risk is caused by the potential entry of air into the reactor. While burning of the graphite is not likely, the air reacts with the surfaces of the fuel pebbles forming CO and CO_2 and thus erodes the protective coating. This would allow activated graphite and radioactive material to leak from the reactor. It is then important to control the amount of air in the vicinity of the reactor. [9, p. 343]

4.3 Reactor modularity

The conventional nuclear power plants generally produce power on the order of 1,000 MW_e. These are expensive to build and it can take a long time for them to return the investment. Another risk of investing into a high-output reactor is the possibility of a reduced need for electricity in the future for example due to economic downturn. While it is possible to run a reactor at below full capacity to follow the energy consumption, it is not as efficient with the older reactors, due to their high fixed costs compared to their variable costs, as with other forms of energy sources. Thus having multiple reactors, that have lower investment costs, with a lower power output are a more flexible option.

One of the aims of PBRs is to make the power plants as modular as possible. This would improve the ease of installing power plants and their quality. The amount and p. 226]cIAEA:HTR10ost of maintenances and the resulting downtimes would be reduced due to the replaceable nature of the modules. [9, p. 340]

This also allows for each power plant to produce power on the order of 100 MW_e yet be viable. This, combined with their lower investment cost and construction time compared to the conventional power plants, makes them a useful resource. An example of an application for PBRs is in the production of hydrogen gas through the use of an intermediate helium cycle [9, p. 331].

4.4 HTR-10

The efficiency of HTRs and their ability of producing heat for industrial processes was noted in China when they began their research. Thus, to verify the safety features and technical viability of modular HTRs, the development of HTR-10 began. [5, p. 226]

The HTR-10 is designed to rely more on passive, inherent safety than the conventional redundant and varied active systems. Thus one of its aims was to prove the concept of inherently safe reactors to the governments and the general public. [5, p. 226]

4.4.1 Core

The core vessel of the HTR-10 is a cylindrical steel structure with a radius of 90 cm and a height of 197 cm. Its bottom is conical with an angle of 30°and is used to help the pebbles exit the core with gravity. The core houses a pebble bed consisting of a 57:43 mixture of fuel pebbles and dummy pebbles respectively with 27,000 pebbles in total during full load. [21, p. 27]

The fuel pebbles are dropped from above into the core and form a conical pile at the top. They move down the reactor and are removed through central channel on the bottom and either recycled back into the reactor or removed as waste if they have reached their target burnup of 87 GWd/t_{HM}. [21, p. 27–28]

The core vessel is surrounded by graphite reflectors. There are ten control rods, seven absorber pebble and three experimental channels, as well as 20 channels for the coolant, through the graphite layers. [21, p. 28]

The reactor uses helium as a coolant, which flows down through the pebbles. Its inlet temperature is 250 °C and it warms up to a temperature of 700 °C. Helium is used due to its stability and chemical neutrality. The coolant flows to the steam generator and comes back up through helium channels in the graphite reflector.

4.4.2 Fuel

The fuel pebbles of the HTR-10 consist of a graphite matrix with a radius of 2.5 cm covered by a 0.5 cm thick fuel-less graphite layer. This graphite acts both as a containment for the fuel particles and a moderator in addition to the dummy pebbles. They have the same total radius as the fuel pebbles, 3.0 cm, but do not contain anything other than graphite. [5, p. 235]

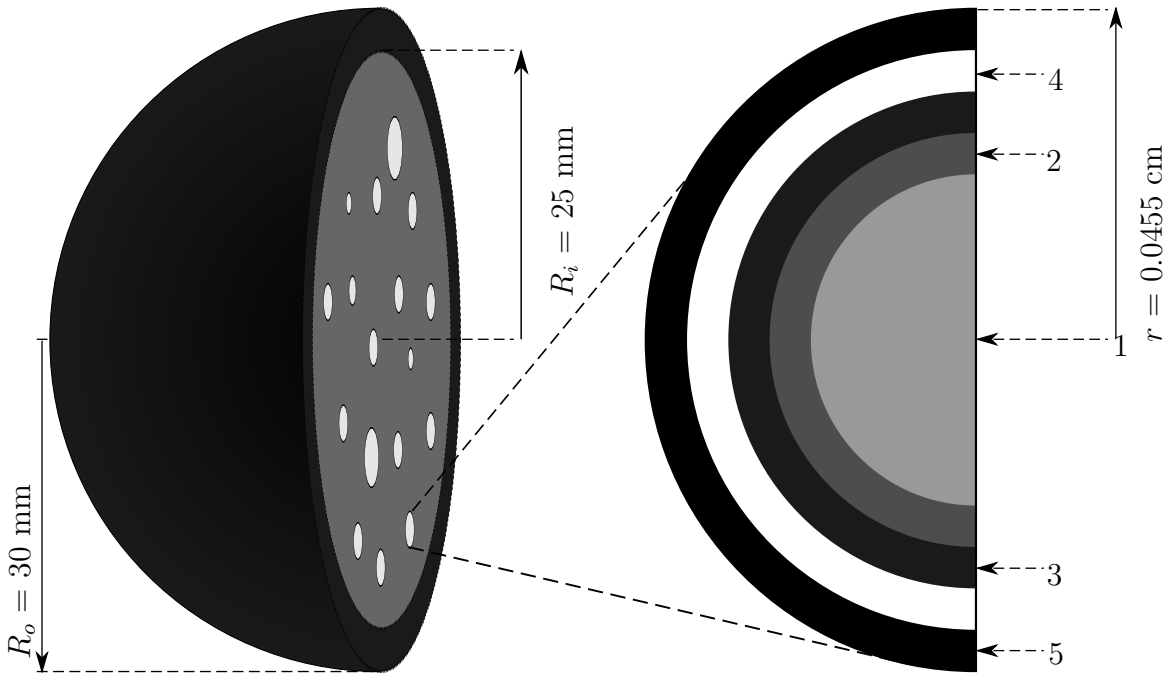

Figure 4.4: The structures of fuel pebbles and TRISO-particles.

Each fuel pebble contains 8,335 TRISO coated fuel particles. These particles contain 5 g of uranium enriched to 17 % U-235. The successive layers are numbered in order from 1 to 5 in figure 4.4. The TRISO coated particles have (1) a kernel of uranium dioxide (UO_2) with a radius of 0.025 cm. Surrounding the kernel is (2) a coat of buffer graphite with a thickness of 0.009 cm. This is followed by (3) an inner layer of pyrolytic carbon (iPyC) 0.004 cm thick. Next is (4) a 0.0035 cm layer of silicon carbide (SiC) followed by (5) the outermost layer of pyrolytic carbon (oPyC) with a thickness of 0.004 cm. [5, p. 229, 235]

The porous buffer layer is designed to hold gaseous fission products and surrounding it is the dense iPyC layer to hold them in. The silicon carbide layer is ceramic and is designed to, in theory, be able to retain any fission products during stress caused by

for example high temperatures.

This coating has been found to have a few sources for particle failure. One of these failures is caused by the build-up of internal pressure. As the particle is irradiated inside the reactor, the gaseous fission products increase the pressure against the silicon carbide layer. Once the build-up is high enough, the layer breaks and causes the rest of the coating to fail with it. [4, p. 11]

A second mechanism of coating failure is the weakening of the SiC through interactions with the fuel kernel given the transport of carbon due to temperature differences within the particle. Additionally the SiC can become porous at higher temperatures and react chemically with fission products. These can, however, be avoided through design choices. [4, p. 12–13]

4.4.3 Safety

The high temperature reactors possess many features that improve their safety. The graphite used as the moderator has a high heat capacity. This allows the core to absorb more thermal energy released before overheating. Other features include the chemically inert fuel, moderator and coolant, the coated fuel particles that are adept at retaining the fission products and the negative thermal coefficient of reactivity the reactor possesses.

The reactor is able to remove the decay heat passively. In the case of a loss of coolant accident (LOCA), the structure of the core is able to conduct and radiate the heat into the surroundings. This heat is then circulated through water inside coolers installed on the walls of the reactor building, which transfer the heat into the atmosphere. [21, p. 30]

The power density inside the reactor core is low, on average it is approximately 2 MW/m^3. This means that the highest temperature reachable by the fuel, during a LOCA and a loss of pressure, will not reach the highest allowed, that is 1,600 °C. [21, p. 27, 30]

Chapter 5

HTR-10 model

The Serpent model of the HTR-10 reactor is discussed in this chapter. The structures of the vessel and the reflector are explained as well as the assumptions and simplifications made to the model. Additionally, a description of a rectangular surface type, that is needed and was added to Serpent, is given.

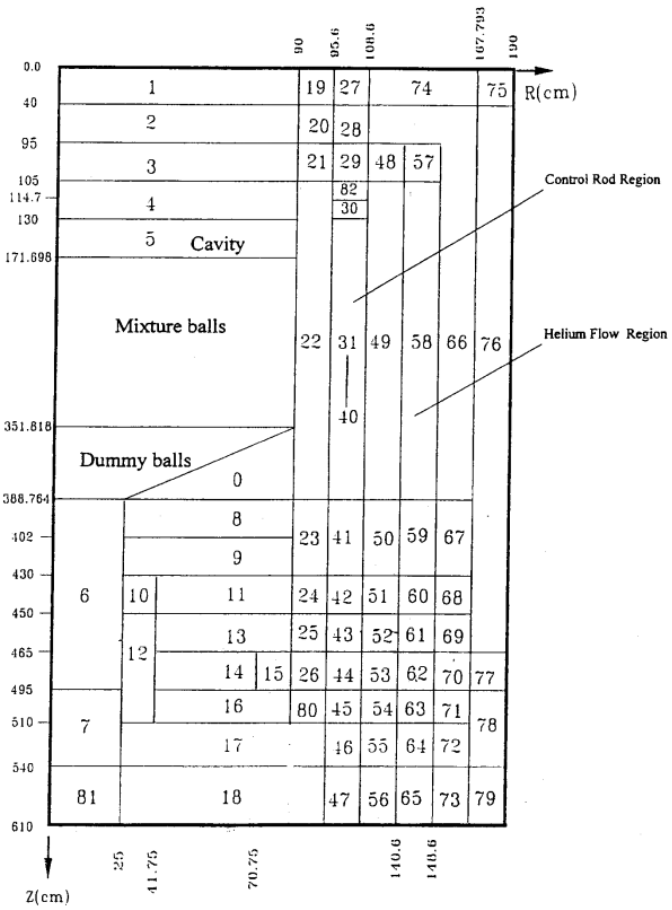

Figure 5.1: Cross-section of the HTR-10 reactor model. [5, p. 241]

Unlike other Monte Carlo reactor physics codes, the Serpent is capable of using discrete coordinates as the locations of pebbles and particles. As such, methods like DEM can be used in conjunction with the code in order to produce realistic pebble beds. As mentioned in section 3.3, this has not been possible with older codes, which rely on lattices for their distribution.

A cross-section of the structure of the reactor is shown in figure 5.1 [5, p. 241]. The core consists of the air cavity and the ball mixture and dummy ball zones. Beneath these is the exit pipe, which includes the zones 6, 7 and 81. This pipe is filled with dummy pebbles, which represent used fuel being removed from the reactor and have the same dimensions as the fuel pebbles but are only filled with graphite. Surrounding these are the reflector zones.

5.1 Reactor vessel

The reactor core is simplified to a cylinder with a conical bottom. The exit pipe is filled with dummy pebbles in the detailed model and they are replaced with graphite blocks in the simplified model. The conus is likewise filled with dummy pebbles and the reactor cylinder has a mixture of fuel and dummy pebbles with a 57:43 fuel to dummy ratio.

These pebbles are randomly distributed in the reactor by dropping them from above. Their interactions are then simulated with discrete element method (DEM) to find the final positions of the pebbles. The generation of these distributions was done by Heikki Suikkanen [16]. The DEM process takes the interactions of the pebbles into account while they settle in the heap after being dropped. Each of the pebbles in the core are thus individually modelled to find their final positions. This results in a central conical heap of pebbles as shown in figures 5.2 and 5.3. This distribution is then made denser through shaking the pebbles. The remaining space inside the reactor is filled with air at room temperature of 27 °C.

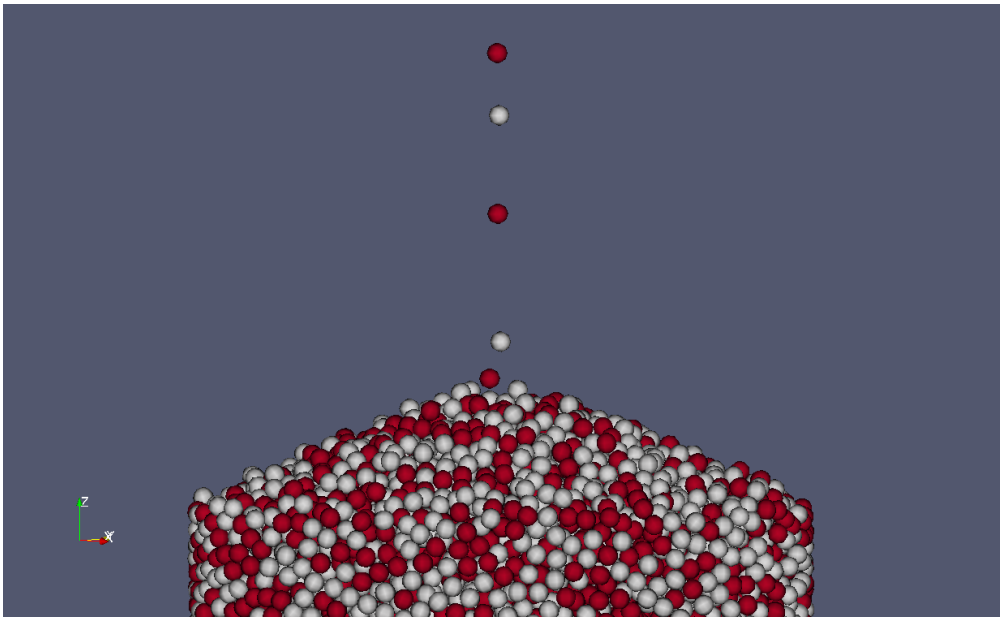

Figure 5.2: Snapshot of the pebble drop process at 16,894 fuel-dummy pebbles combined.

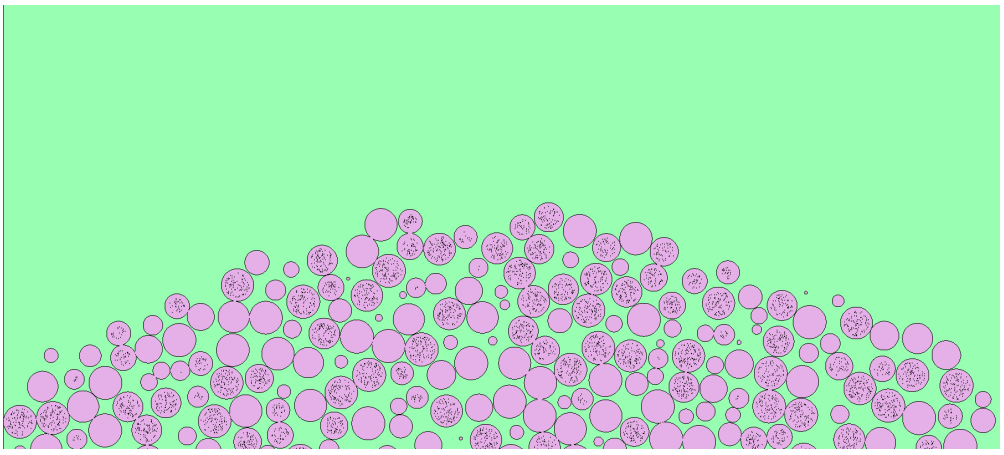

Figure 5.3: Cross section of the top of the bed with 17,941 pebbles after the pebbles have settled.

10 different fuel particle distributions are used with the fuel pebbles to alleviate possible errors from having identical fuel pebbles. These are random distributions generated with Serpent. The fuel particle distributions are selected randomly for each fuel pebble.

The modelling of fuel thus differs significantly from the prior studies, where regular lattices were used [5] [1]. In Serpent it is possible to use discretely defined positions for the pebbles and particles. It is thus possible to produce more accurate results due to the lack of a need to place the pebbles in lattices.

5.2 Reflector

The reflector consists mostly of boronated carbon blocks. These blocks are passed through by twenty helium channels, thirteen channels for irradiation and control rods, seven channels for small absorber balls, KLAKs (KLeine Aufsauger Kugeln), and a hot gas duct.

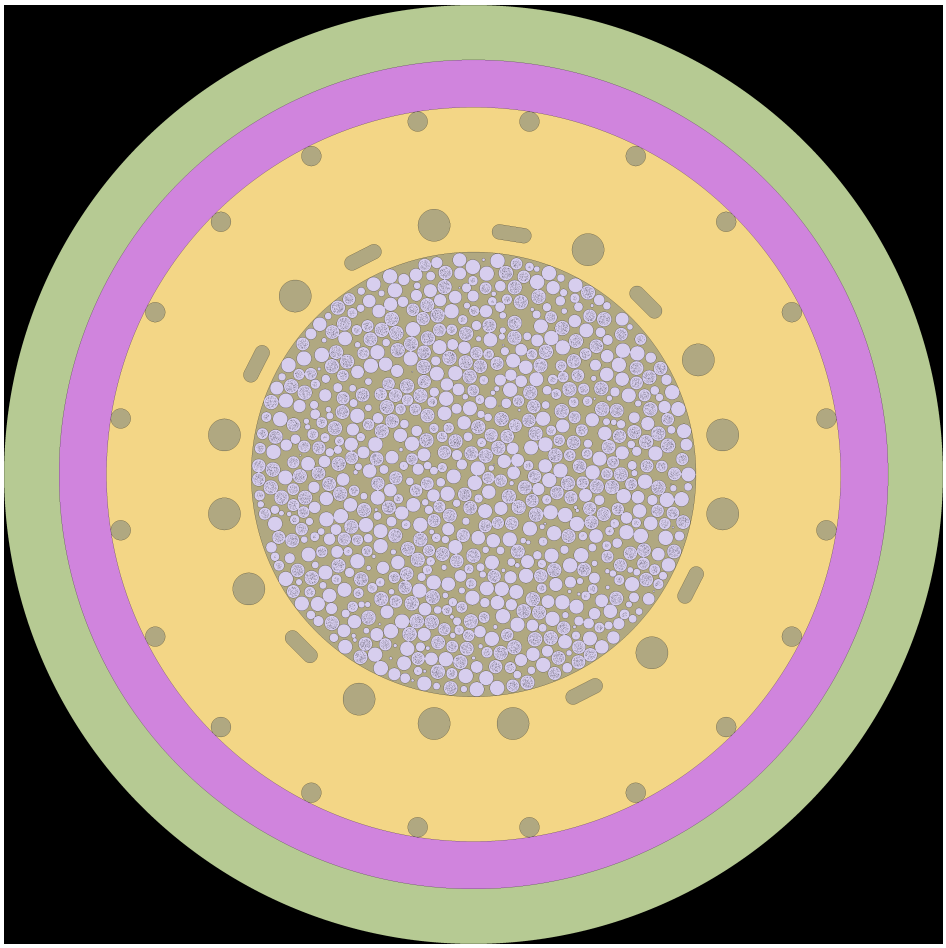

Figure 5.4: A cross-section of the reactor with the surrounding reflector.

In the figure 5.4 the control rod and irradiation channels surround the core along the inner circle. Alongside with them are the elliptical KLAK channels. The channels along the outer circle are the helium coolant channels. In the model all of the aforementioned channels are filled with saturated air at room temperature.

5.3 Elliptical KLAK channels

The HTR-10 reactor has seven elliptical KLAK channels. The geometrical model of the cross section of these channels is a rectangle with semicircular ends. This type of a surface is unfortunately not supported by the pre-existing surfaces in Serpent [12]. The only rectangular surface is a square cylinder that can not be rotated.

Surface cards are used by Serpent to determine the boundaries of material cells. A cell is defined to be the space inside each of its defining surfaces. A point in space is inside a surface if the solution of the equation of the surface at that point is negative. Each added defining surface then adds a new check in the calculations. It is then beneficial to keep the amount of defining surfaces as low as possible and thus it is preferable to create a custom surface if the alternative is to use multiple other surfaces. In this case a new, elliptical surface avoids the need to use a number of circular cylinders and planes to achieve the same goal.

The new surface, `RECTZ`, can be used to create a rectangle at any angle with optional rounded corners that can be used to make its ends semicircular. The input of the surface is

```
RECTZ x0 y0 l h [sin(phi) cos(phi) r0],
```

where `x0`, `y0` are the centre coordinates, and `l`, `h` are the length and height of the rectangle respectively, and are the only required inputs. The other inputs are optional, where `sin(phi)` and `cos(phi)` are the sine and cosine of the angle of rotation about the z-axis and `r0` is the rounding radius.

If the rectangle is not located at the origin, it is moved there using the `x0` and `y0` input coordinates. Following this the rectangle is rotated anticlockwise using the sine and cosine inputs to align the length with the x-axis and the height with the y-axis. The necessary checks for neutrons are done similarly to the `SQC` surface with the constant radius replaced with the length and height.

The cross-sectional surface area of the rectangle is calculated with the formula

$$A_c = 4lh - (4 - \pi)r_0^2, \tag{5.1}$$

where A_c is the cross-sectional area. The maximum dimensions for the x- and y-coordinates of the surface are also calculated. Since the rectangle is symmetrical, the maximum distances between the surface and its centre are same for both the positive and the negative directions along the x- and y-axes. These distances are

$$\begin{aligned} d_x &= h|sin(\varphi)| + l|cos(\varphi)| \\ d_y &= h|cos(\varphi)| + l|sin(\varphi)|, \end{aligned} \tag{5.2}$$

where d_x and d_y are the maximum distances along the x- and y-axes respectively and φ is the angle between the x-axis and any line parallel to the sides of the rectangle with the length l. These distances are derived from the figure 5.5.

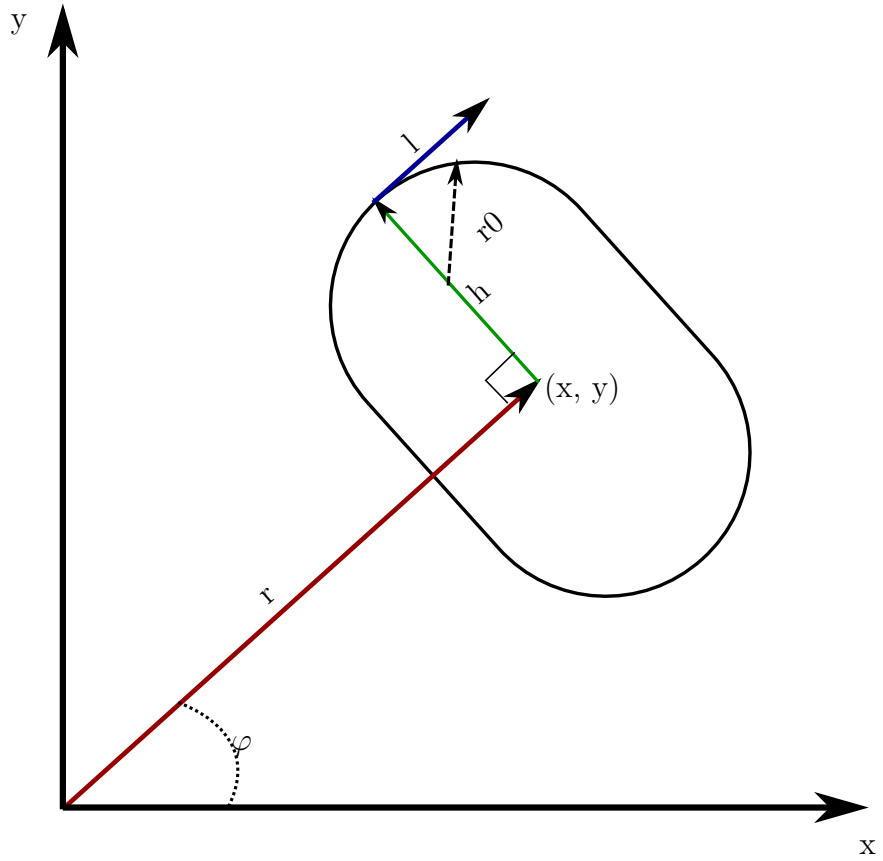

Figure 5.5: The dimensions required to plot a rotatable rectangle.

5.4 Simplifications and assumptions

Modelling an exact copy of the physical reactor is not possible nor practically feasible due to the resulting complexity of the model and consequently the required computation time. Additionally, some materials of the structure have insignificant to no effect on the operation of the reactor, for example the reactor vessel, which composed of stainless steel. Due to the lack of detailed public material data, the material composition of the core is assumed to follow those reported by IAEA (International Atomic Energy Agency). [5]

Some structural shapes are too complicated to be simulated using the available surfaces. An example of such a case are the conical extensions in the conus of the reactor. In cases such as these, they are omitted and replaced with the nearest equivalent surface type, which in this case is a cone.

The worths of control rods are not simulated in the model. The control rod channels are present but filled with air. In addition, in the simplified case some of the dummy pebbles below the conus are replaced with graphite blocks.

5.5 Prior studies

There have been a number of studies in the past that have simulated the initial criticality of the HTR-10 reactor. In this section a few such studies are listed along with their results. These will be later used to compare the results received from Serpent to determine the differences.

The chosen studies were done in China using VSOP and MCNP4A codes [5, p. 246–247], France using TRIPOLI4 [5, p. 301], Germany using VSOP code [5, p. 309], USA using MCNP4B [5, p. 283] and Iran using MCNP5 [1, p. 282]. They are shown in the table 5.1.

In the Chinese MCNP4A study the fuel discharge tube was omitted. The fuel particles inside the pebbles were generated within a hexahedron lattice using an edge length of 0.19876 cm. The fuel pebbles are arranged in a hexagonal lattice horizontally and a simple cubic (SC) lattice vertically. The calculation was done using 5 skipped cycles and 140 active cycles with 10,000 source neutrons each. [5, p. 245–246]

The study done in USA took the double heterogeneity of the TRISO particles and the pebbles into account and used an explicit model of the reflector. However, like in the Chinese study, an explicit modelling of the pebbles in the reactor was not possible due to the limitations of MCNP and they had to be approximated into a body-centred cubic (BCC) lattice. Additionally, it was not possible to model the moderator pebbles of the same size as the fuel pebbles due to lattice limitations. The fuel particles were distributed within the pebbles inside the SC lattice. The calculation used 1 million source neutrons. [5, p. 281–282, 287]

In the Iranian study the TRISO particles are generated inside the pebble in a hexahedral lattice, followed by moving them in a random direction up to a distance of 0.0515 cm. The fuel pebbles were inserted into the core by randomly generating their locations in a chosen volume and iterating until there were no overlaps by moving the intersecting pebbles away from each other. The calculation included 50 skipped cycles and 500 active cycles with 10,000 source neutrons each. [1, p. 278–280]

Table 5.1: Results from prior studies on the criticality of HTR-10.

Study	Code	Library	T [K]	Pebbles	k_{eff}	Note
China[a]	VSOP	ENDF/B-V, JEF-1	300	16,470	0.98216	
				17,294	1.00060	
				17,267	1.00000	Interpolated
	MCNP4A	ENDF/B-V	300	17,109	1.00000	Interpolated
France[a]	TRIPOLI4	JEF-2.2	293	16,108	1.00000	
Germany[a]	VSOP	ENDF/B-V, JEF-1	293	17,389	1.00000	Interpolated
USA[a]	MCNP4B	ENDF/B-VI	300	16,906	1.00000	
Iran[b]	MCNP5			16,890	1.00032	

[a] IAEA [5].
[b] Abedi, Vosoughi [1].

Chapter 6

Cases

This chapter contains brief descriptions of the study cases and the reasons behind them. Two cases are studied in total, with some differences as explained below.

In both cases the reference test with 16,890 pebbles at a 57:43 fuel-dummy ratio is first repeated to find out the coefficient of multiplication of the reactor. Following this, the amount of pebbles required to reach criticality is determined. The calculations are run on a modified Serpent 2.1.21 where the elliptical surface was added in order to properly model the KLAK channels. The material cross-section libraries used in both cases are ENDF/B-VII, JEFF-3.1.1 and JENDL-4; and the temperature of the reactor is 300 K. The thermal scattering libraries used are ENDF/B-VII for the ENDF/B-VII and JENDL-4 material libraries, and JEFF-3.1 for JEFF-3.1.1.

Due to the differences in the JENDL-4 library compared to the other nuclear data libraries, some of the materials had to be changed due to their absence. The isotopes 6000, carbon; 14000, silicon; and 18036, argon, were replaced with 6000, 14028 and 18000 respectively. In addition, the thermal scattering isotope for graphite was changed from 6012 to 6000.

In most of the calculations 20 skipped and 1,000 active cycles are used. Each cycle has a source neutron population of 600,000 combining to a total of 600 million neutron histories. The calculations are parallelised into two tasks, each with sixteen threads. As exception to these are simulations with 17,941 and 17,947 pebbles in the cases of the detailed ENDF/B-VII and simplified JEFF-3.1.1 simulations. They have double the amount of active cycles and tasks in order to receive results that are not within the error margin of each other.

The reactor is split into 17 universes. The reactor vessel and the exit pipe are split into four quadrants using horizontal planes at the top of the reactor vessel, at the bottom of the conus and above the hot gas duct.

In the first case the dummy pebbles of zones 7 and 81 are modelled explicitly. This was not done in the reference but they were simplified to graphite bricks. An illustration of the reactor in the first case is shown in figure 6.1.

However, the simplification of the lower dummy pebbles is done in the second case to compare the results to the prior studies and to see the magnitude of the effect of simplifying the model. The only difference to the first case is the replacement of the bottommost dummy pebbles with graphite. The same pebble distribution applies for the rest of them in both cases. This means that some of the pebbles will get cut but the effect should be negligible. The cross-section of the reactor in the second case can be seen from figure 6.2.

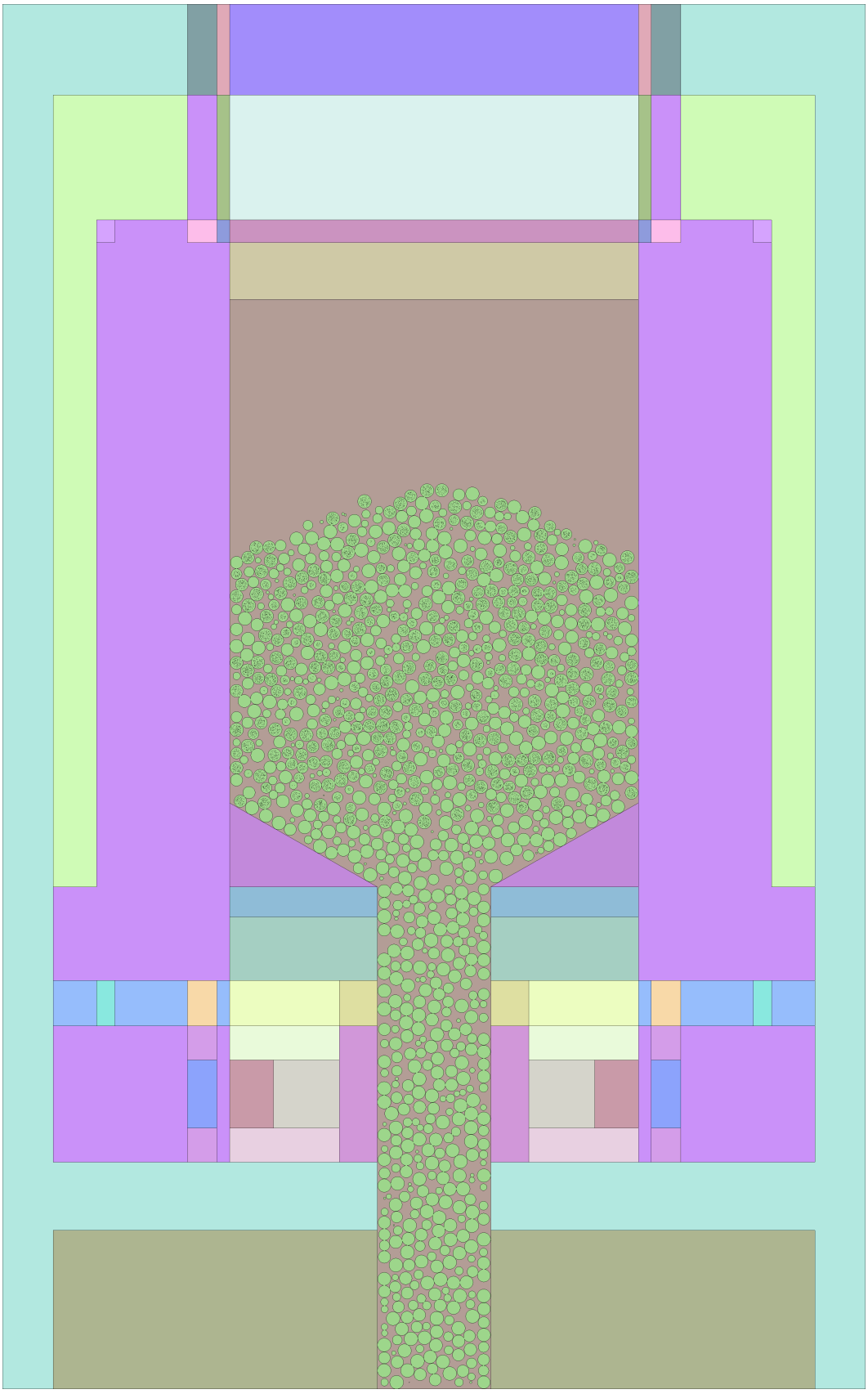

Figure 6.1: A vertical cross-section of the detailed reactor with the surrounding reflector.

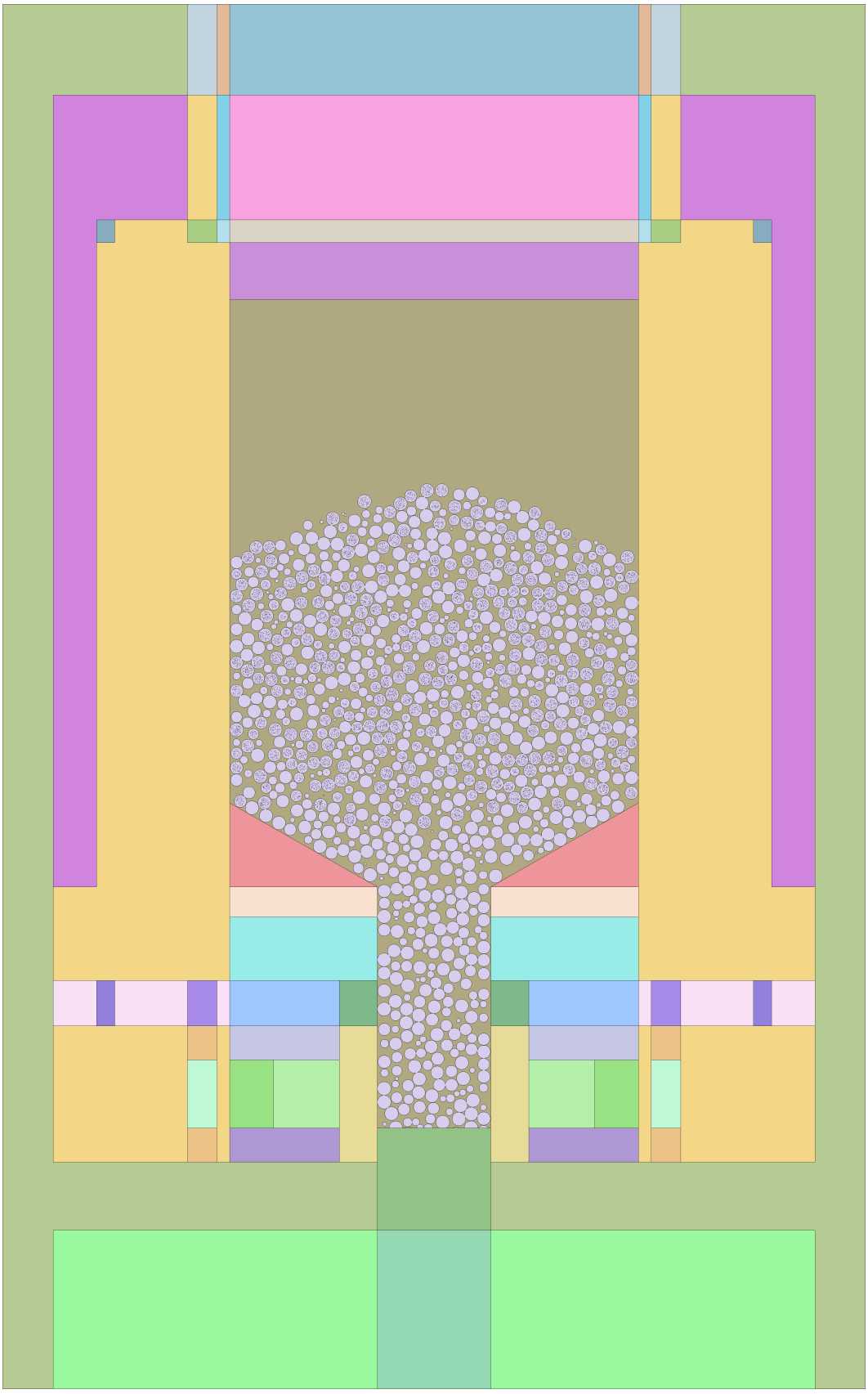

Figure 6.2: A vertical cross-section of the simplified reactor with the surrounding reflector.

Chapter 7

Results

This chapter includes the results of the aforementioned cases. Included are the simulation results alongside cross sections of the core and the neutron flux distribution. In addition, the results received from additional calculations are listed for further analysis.

7.1 Case 1

The calculation results from the simulations with 16,890, 17,941 and 17,947 pebbles are shown in the table 7.1. Most of these calculations took approximately 15 hours, producing 600 million neutron histories. The exceptions were the 17,941 and 17,947 -pebble simulations using the ENDF/B-VII library, which used 1,200 million neutron histories.

Table 7.1: Results of the first case with the detailed reactor.

Core	Pebbles	$k_{\text{eff}} \pm \sigma$ Serpent 2.1.21 ENDF/B-VII	$k_{\text{eff}} \pm \sigma$ Serpent 2.1.21 JEFF-3.1.1	$k_{\text{eff}} \pm \sigma$ Serpent 2.1.21 JENDL-4
1	16,890	0.97734 ± 0.00005	0.97758 ± 0.00005	0.97020 ± 0.00005
2	17,941	0.99971 ± 0.00004	0.99996 ± 0.00005	0.99255 ± 0.00005
3	17,947	0.99980 ± 0.00004	1.00006 ± 0.00005	0.99265 ± 0.00005

Illustrations of the neutron flux distribution in the pebble beds of the first case can be seen from figures 7.1 and 7.3. Similarly the geometries of the reactor are shown with cross sections in figures 7.2 and 7.4.

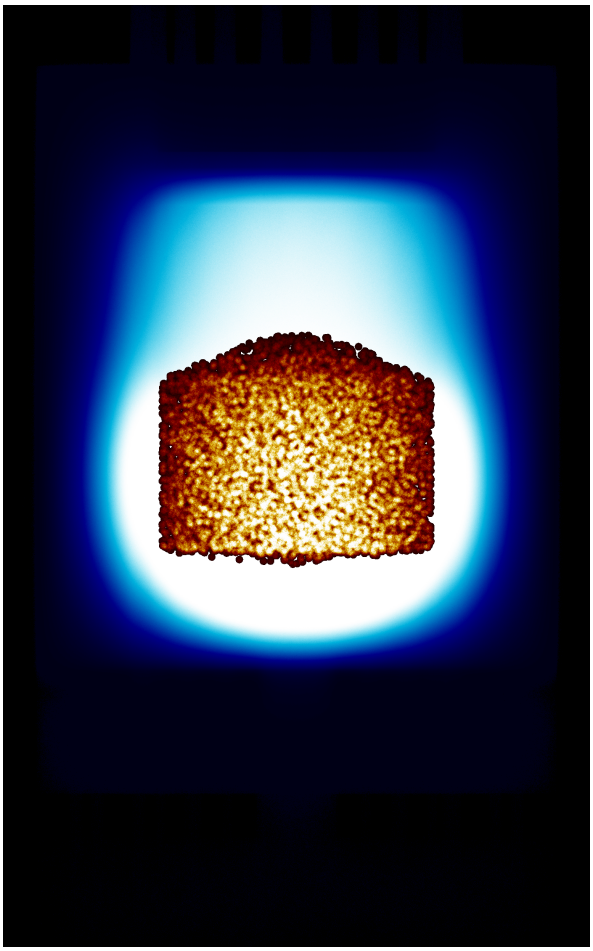

(a) Vertical cross section.

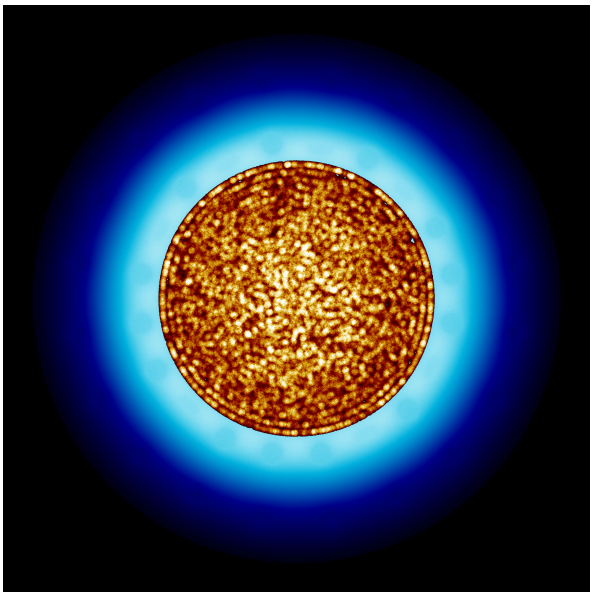

(b) Horizontal cross section.

Figure 7.1: The neutron flux distributions with 16,890 pebbles in the first case.

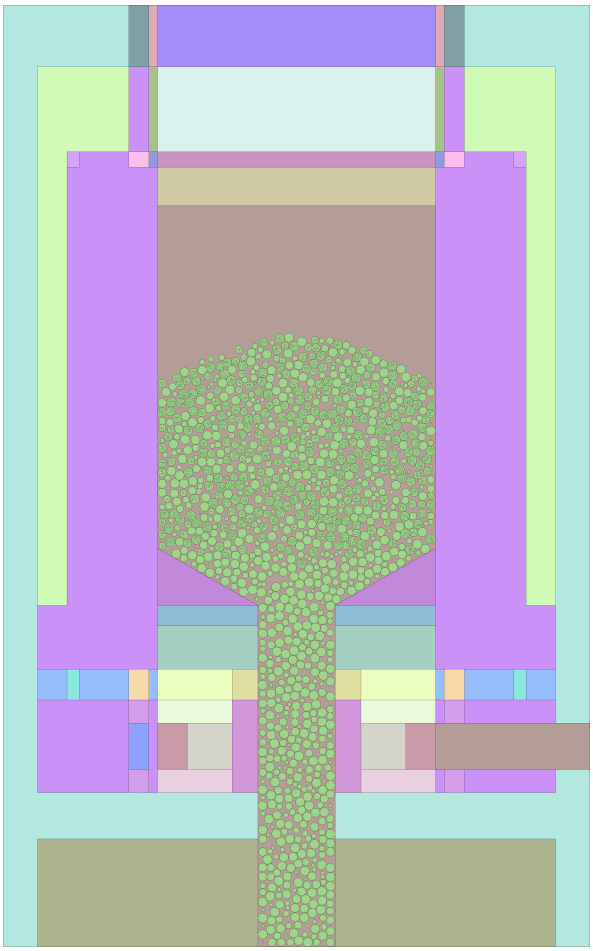

(a) Vertical cross section.

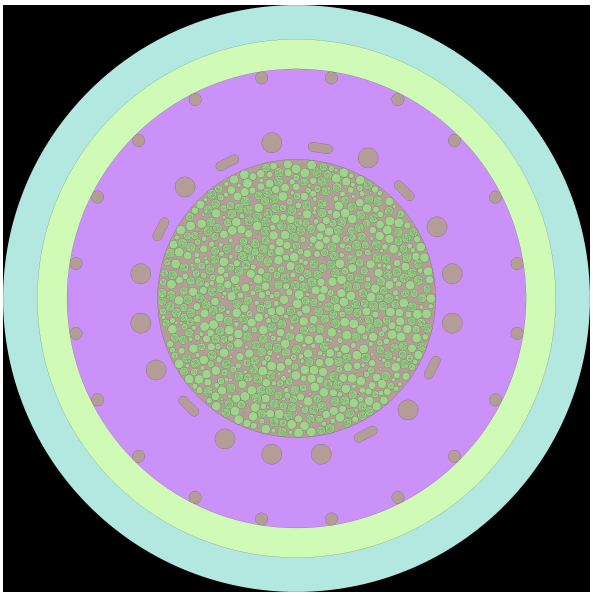

(b) Horizontal cross section.

Figure 7.2: The geometry cross sections with 16,890 pebbles in the first case.

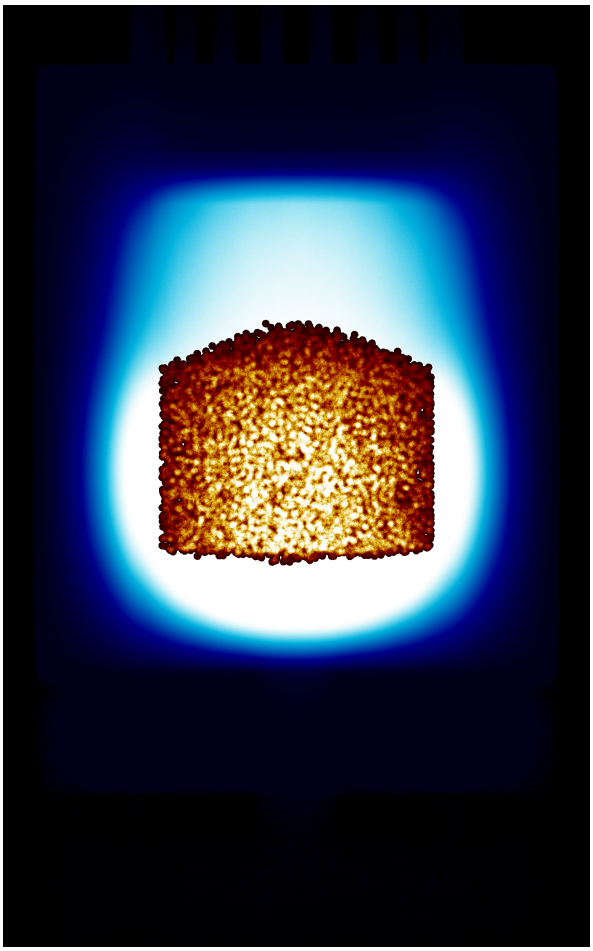

(a) Vertical cross section.

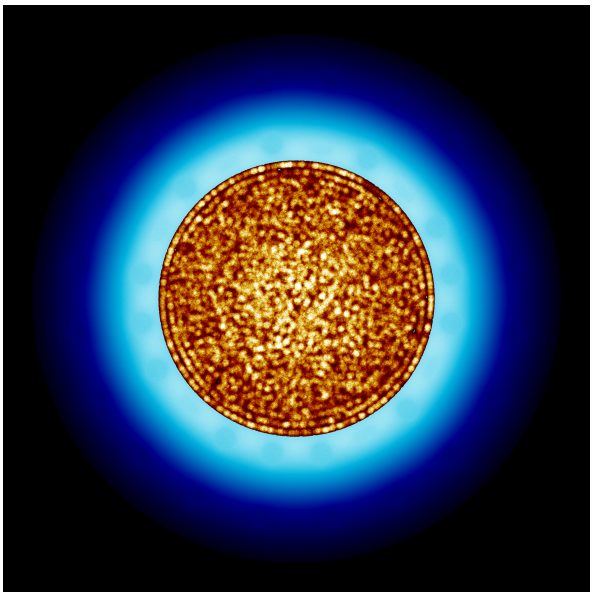

(b) Horizontal cross section.

Figure 7.3: The neutron flux distributions with 17,947 pebbles in the first case.

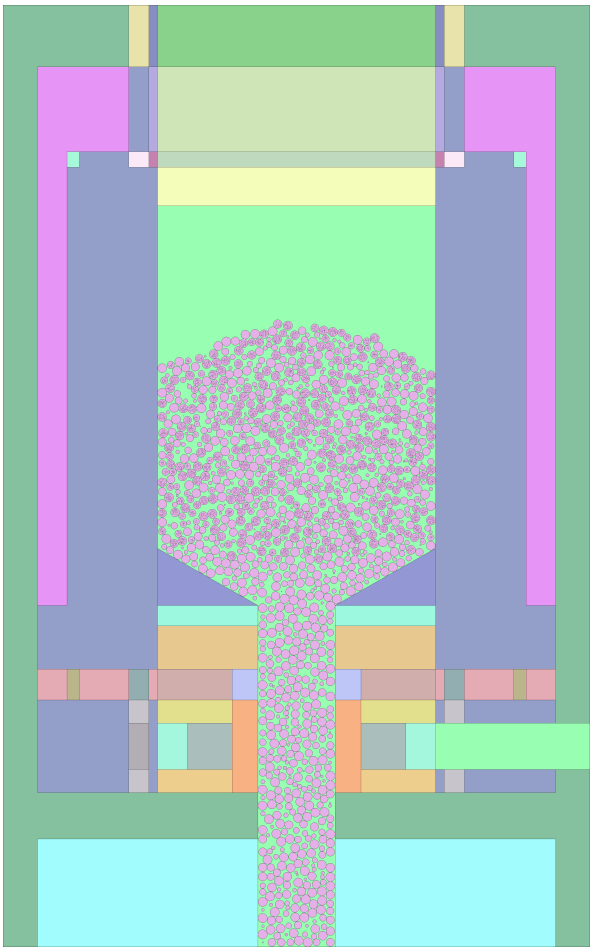

(a) Vertical cross section.

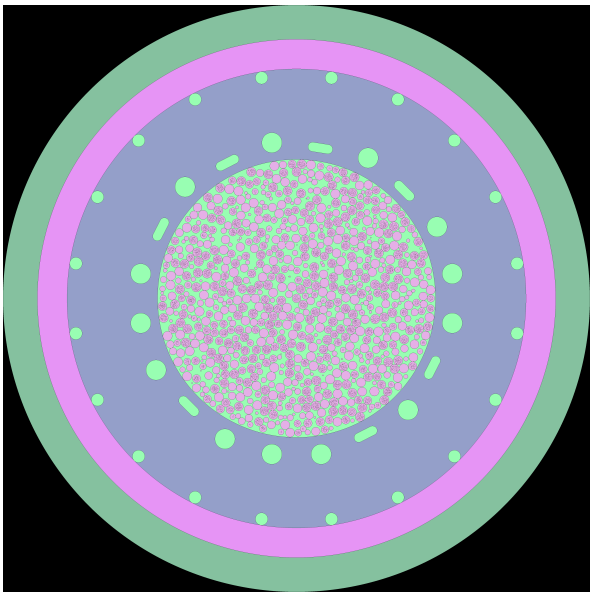

(b) Horizontal cross section.

Figure 7.4: The geometry cross sections with 17,947 pebbles in the first case.

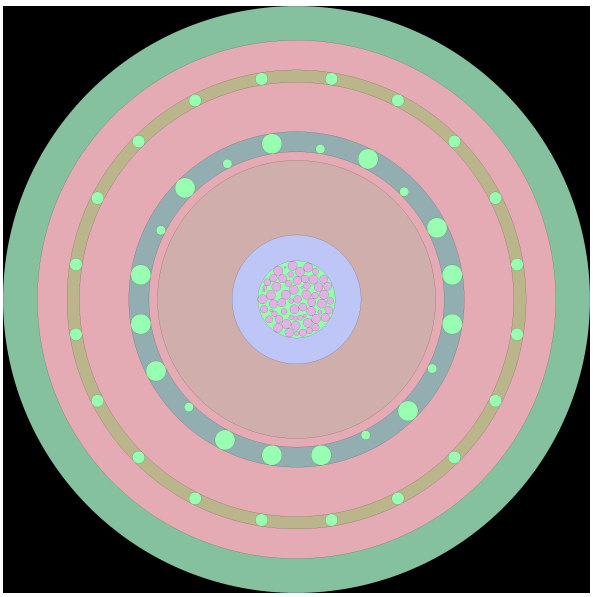

(a) Horizontal cross section at z=-440 cm.

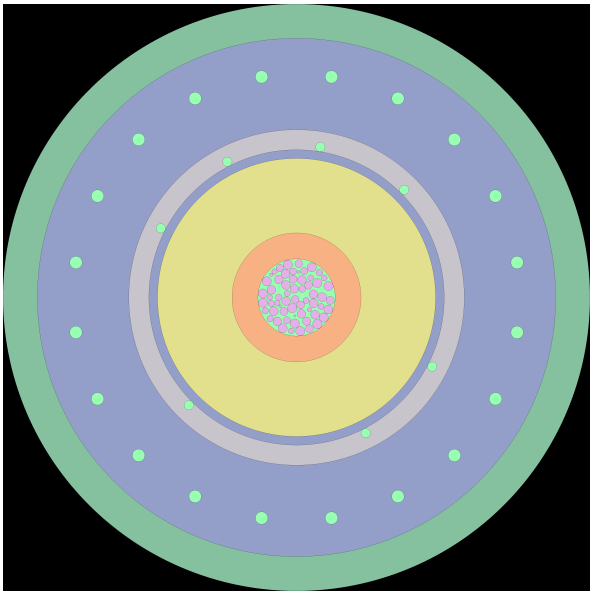

(b) Horizontal cross section at z=-502.5 cm.

Figure 7.5: The geometry cross sections of the lower part of the core with 17,947 pebbles in the first case.

7.2 Case 2

The results of the second case, calculated again with 16,890, 17,941 and 17,947 pebbles. These results are displayed in the table 7.2. The calculations took approximately 15 hours and used 600 million neutron histories each to produce the results. The exceptions here were the 17,941 and 17,947 -pebble simulations using the JEFF-3.1.1 library, which used 1,200 million neutron histories.

Table 7.2: Results of the second case with the simplified reactor.

Core	Pebbles	$k_{\text{eff}} \pm \sigma$ Serpent 2.1.21 ENDF/B-VII	$k_{\text{eff}} \pm \sigma$ Serpent 2.1.21 JEFF-3.1.1	$k_{\text{eff}} \pm \sigma$ Serpent 2.1.21 JENDL-4
1	16,890	0.97726 ± 0.00005	0.97744 ± 0.00005	0.97024 ± 0.00005
2	17,941	0.99980 ± 0.00005	1.00001 ± 0.00004	0.99244 ± 0.00005
3	17,947	0.99984 ± 0.00005	1.00007 ± 0.00004	0.99263 ± 0.00005

Figures 7.1 and 7.3 show the neutron flux distribution in the simplified case with 16,890 and 17,947 pebbles respectively. Likewise the figures 7.2 and 7.4 display the cross-sectional structures of the reactor beds with the aforementioned pebble counts.

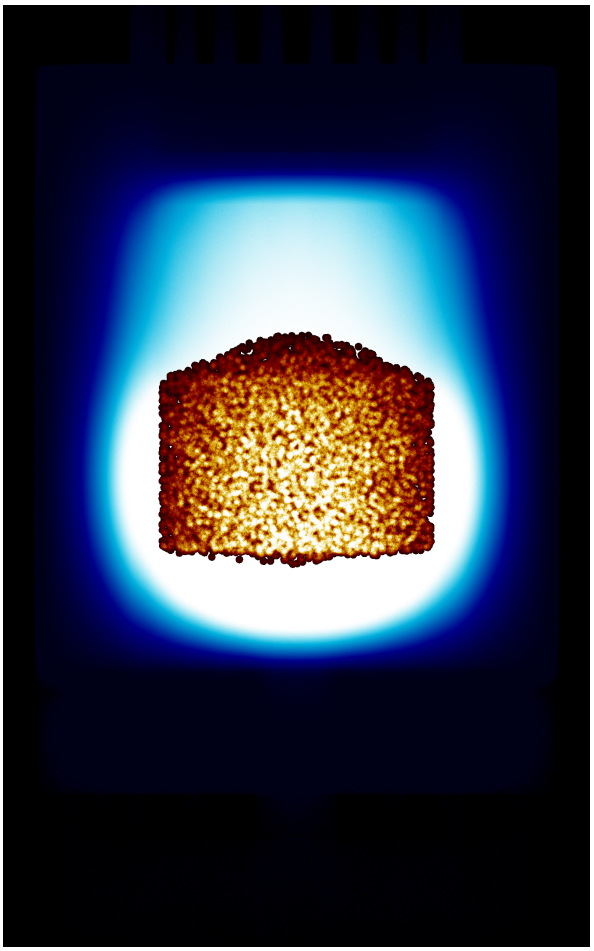

(a) Vertical cross section.

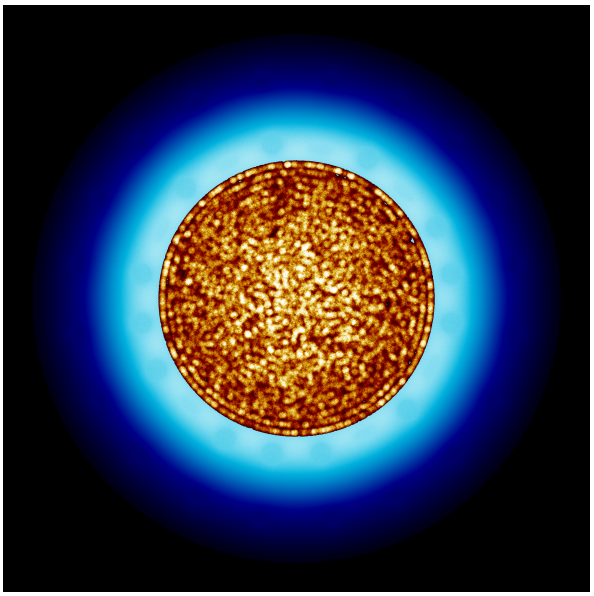

(b) Horizontal cross section.

Figure 7.6: The neutron flux distributions with 16,890 pebbles in the second case.

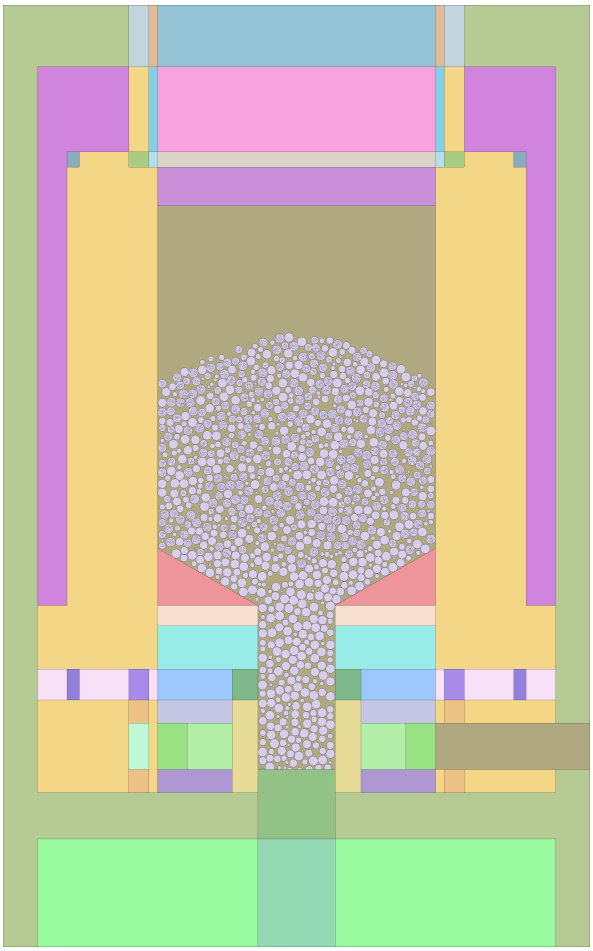

(a) Vertical cross section.

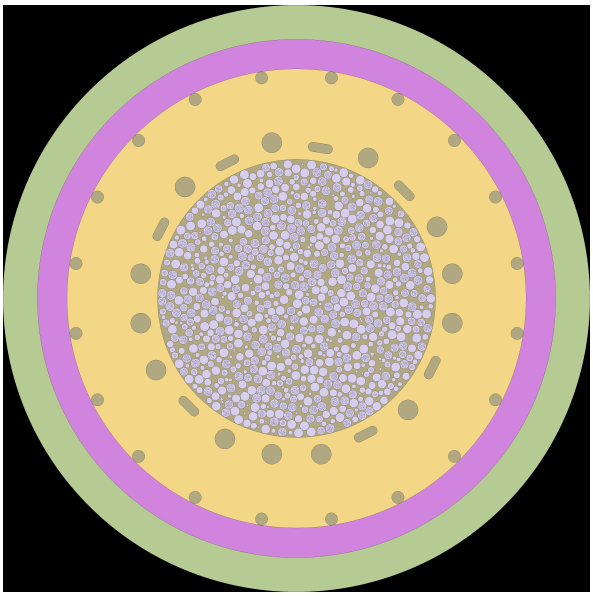

(b) Horizontal cross section.

Figure 7.7: The geometry cross sections with 16,890 pebbles in the second case.

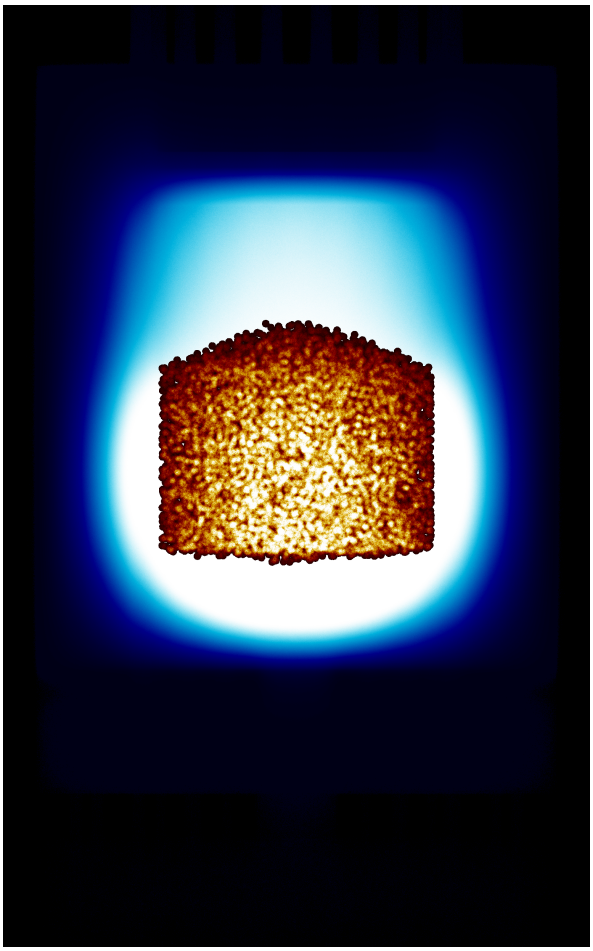

(a) Vertical cross-section.

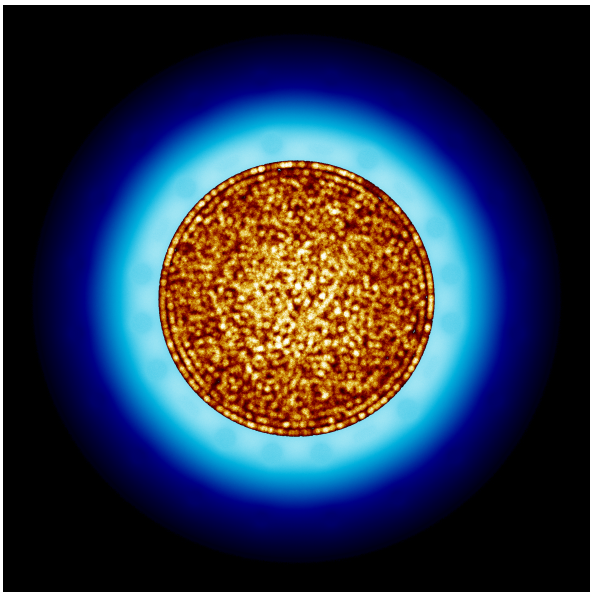

(b) Horizontal cross section.

Figure 7.8: The neutron flux distributions with 17,947 pebbles in the second case.

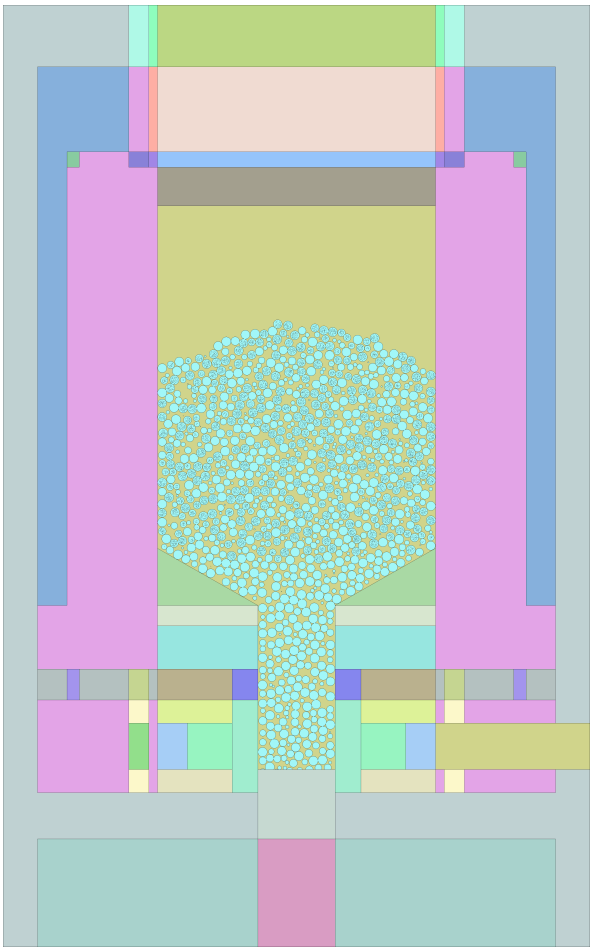

(a) Vertical cross section.

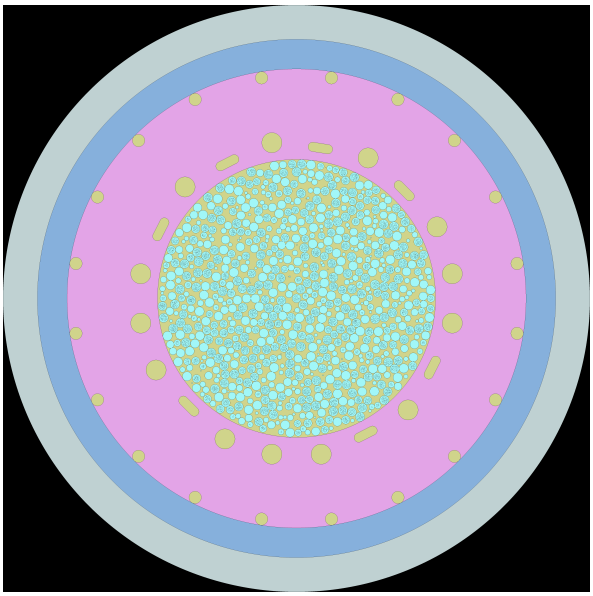

(b) Horizontal cross section.

Figure 7.9: The geometry cross sections with 17,947 pebbles in the second case.

7.3 Other results

During the calculations of the cases, the following results were also received for further analysis of the cases. In the table 7.3, a comparison between results received using JEFF-3.1 and ENDF/B-VII thermal scattering libraries with the ENDF/B-VII material library is shown.

Table 7.3: Results of the comparison between the JEFF-3.1 and ENDF/B-VII thermal scattering libraries while using the ENDF/B-VII material cross section library.

		Case 1		Case 2	
		k_{eff}	k_{eff}	k_{eff}	k_{eff}
		Serpent 2.1.21	Serpent 2.1.21	Serpent 2.1.21	Serpent 2.1.21
Core	Pebbles	ENDF/B-VII	JEFF-3.1	ENDF/B-VII	JEFF-3.1
1	16,890	0.97734	0.97766	0.97726	0.97773
2	17,941	0.99984	1.00012	0.99980	1.00003
3	17,947	0.99982	1.00015	0.99984	1.00022

In addition, a single simulation was performed to determine the effect enabling the Doppler Broadening Rejection Correction (DBRC) has on the resulting multiplication coefficient. The result from this simulation, compared with an earlier result where it was disabled, is shown in table 7.4.

Table 7.4: Comparison of the results of a simulation using the DBRC to the same simulation with it disabled.

		k_{eff}	k_{eff}
		Serpent 2.1.21	Serpent 2.1.21
		ENDF/B-VII	ENDF/B-VII
Core	Pebbles	DBRC enabled	DBRC disabled
1	16,890	0.97730	0.97734

Chapter 8

Discussion

In this chapter the HTR-10 model and its development are first discussed. Following this are the discussions involving the results and their error analysis. Finally, some suggestions for possible future developments for the improvement of these results are given.

8.1 Model

Initially the elliptical KLAK channels were modelled using basic surface types such as cylinders, planes and pads. This, however, lead to an excessive number of cells in the vicinity of the channels. They required six surfaces each, four planes to form the rectangular midsection and two cylinders at each end. Due to the lack of additions, subtractions and complements with surfaces in cell definition in Serpent, the required number of cells would have been significantly higher than with MCNP. In addition there were no valid rectangular surface types that could have been used with cylinders to form the required elliptical cylinders. The only square cylinder surface could not be rotated and thus was not viable for use to form the rectangles from smaller squares.

A new surface type was thus programmed by myself in order to simplify the calculation. It was made to be able to be rotated around the origin, have rounded corners up to semicircular ends and variable side lengths. This allowed the positioning of the required channels without the need of translation cards. This allowed a KLAK channel to be modelled by a single surface and thus only require one cell. Due to the reduced amount of cell checks and consequently surface checks, the time required for the simulation was reduced.

The simplified model is identical to the reference model of the prior studies, where the bottom-most dummy pebbles are approximated with graphite blocks. However, given both of the cases use the same pebble beds, the lowest pebbles in the simplified case can intersect with the graphite block that replaced some of the dummy pebbles.

The detailed model, on the other hand, differs from the reference model since all of the dummy pebbles are explicitly modelled. However, as can be seen from the tables 7.1 and 7.2, the results do not depend much on the modelling of these pebbles except when the JENDL-4 library is used.

The reason for this can be most clearly seen from the neutron flux mesh figures such as 7.1 and 7.3 with the first case or 7.6 and 7.8 with the second case. The neutron flux can be seen to mostly concentrate close to the bed and above it, stopping at the boronated graphite blocks of the reflector. The amount of neutrons that reach the very bottom is relatively low.

8.2 Results

As can be seen from the results in tables 5.1, 7.1 and 7.2, the results received using the Serpent models differ from those of the prior studies with all of the used libraries. With 16,890 pebbles, which is the reference result from the empirical test, the reactors were subcritical by 2,266 pcm with ENDF/B-VII, 2,242 pcm with JEFF-3.1.1 and 2,980 pcm with JENDL-4 in the detailed case. In the simplified case they were subcritical by 2,274 pcm, 2,256 pcm and 2,976 pcm in the same respective order.

The interpolated amount of pebbles to reach criticality in the detailed cases were approximately 17,961, 17,943 and 18,397 for ENDF/B-VII, JEFF-3.1.1 and JENDL-4 respectively. In the simplified cases these amounts were 17,970, 17,940 and 18,177 in the same order. The results for the detailed ENDF/B-VII and simplified JENDL-4 simulations had to be redone with double the amount of neutron histories due to the original results for the 17,941 and 17,947 pebbles were within the confidence interval of each other. A summary of these results, along with those of the prior studies, is shown in the table 8.1.

Table 8.1: Summary of the critical numbers of pebbles.

Library	Case 1	Case 2	China	France	Germany	USA
ENDF	17,961	17,970	17,267 17,109		17,389	16,906
JEFF	17,943	17,940		16,108		
JENDL	18,397	18,177				

The criticality results from the ENDF/B-VII library then differ from those of the prior studies by approximately 600–1,860 pebbles if all of the prior studies are considered or 400–860 if only studies using an ENDF library are considered. With JEFF-3.1.1 these differences are 550–1,830 pebbles for both considerations. Finally, with JENDL-4 the results differ by 1,000–2,290 pebbles in the detailed case and by 780–2,070 in the simplified case.

The results from the detailed cases are generally close to those from the simplified cases, differing by 9 with ENDF/B-VII and by 3 with JEFF-3.1.1. However, with JENDL-4 the difference is a noticeable 220.

8.3 Error analysis

The results differ noticeably from those of the earlier studies. The difference between the results from ENDF/B-VII and JEFF-3.1.1 in this study to those of the prior studies are, nonetheless, rather small. These differences can be caused or affected by multiple factors, which include the effects of the packing fraction of the fuel-dummy pebble mixture, temperature, possible localisation of the moderator in certain areas of the core, the simplification of the model and simulation parameters.

In the prior studies the packing of the fuel-dummy pebble mixture was not random. Instead, they were located within lattices wherein their locations were randomised. This can effect the accuracy of the simulation because the pebbles were dropped from the top of the reactor in HTR-10. The distribution of the mixture and the shape of the pile can thus greatly differ from that of an actual one.

In Serpent this issue is not present. Natural distributions of dropped pebbles are possible to be modelled because their explicit centre coordinates can be used as input regardless of their generation method. It is then possible to generate these distributions

using external codes, such as the DEM-based pebble distribution generator used in this thesis. These distributions are able to represent actual reactor loads more accurately due to the explicit modelling of the pebble to pebble -interactions within the reactor during the dropping phase.

However, due to the random nature of the dropped pebbles, as compared to the ones placed in lattices, the packing fraction of the reactor can vary depending on the distribution. This is true for both the general packing fraction as well as localised differences in pebble density. It is possible to cause areas of higher void fraction than a regularly distributed bed. These areas can cause the multiplication coefficient with a given amount of pebbles to be lower than in the reference results.

The aforementioned irregularity of pebble packing can be seen from the cross sections of the reactors shown in figures 7.2, 7.4, 7.7 and 7.9. There are localised air pockets between pebbles, which could cause negative reactivity due to the reduced moderation.

Another variable is the temperature of the material used in the simulation. In this study the reactor was modelled at a room temperature of 27 °C. The temperatures at which the prior studies were performed were 27 °C for China and USA, 20 °C for France and Germany. Whereas the temperatures are mostly identical, the 7 degree difference between this, the Chinese and the American studies and the others can have an effect on the multiplication coefficient. This effect, however, is expected to be low, lowering the results of the studies using 27 °C by approximately 42 pcm [3, p. 563].

A third source of error is the potential presence of localisations of moderator pebbles inside the reactor. This is similar to the case of the localised increases in void fraction. It is a direct result from the random distribution of the pebbles. When dropped into the reactor the type of the pebble is randomly picked while keeping the 57:43 fuel-dummy ratio constant. They are then allowed to drop and interact freely with each other. It is then possible that certain areas of the reactor contain a significantly higher proportion of moderator pebbles.

This can in particular be seen in the geometry cross sections of chapter 7, for example the figure 7.2a. The fuel pebbles can be seen grouping up in certain areas of the core. Albeit only a cross section of the reactor, it shows the localisation of fuel and moderator pebbles is possible.

In the lattice-based distributions of the other studies the fuel and moderator peb-

bles are also randomly located within the lattice. They imitate the distribution of the actual reactor but are not able to completely replicate the randomness due to the lattice limitations. Thus, while the prior studies are also affected by the localisation of moderator, the regular nature of the lattices reduces the overall randomness of the pebble distribution and thus lessens the effect.

This problem also applies to the distributions of the fuel particles within the fuel pebbles. Whereas the other studies used lattice nodes also inside the pebbles, the distribution generation in Serpent is completely random. Given the smaller differences in the distances within the pebbles, this can have a little to no effect. To help diminish this effect, 10 different particle distributions were used in this study, unlike the prior studies where a single distribution is mentioned to have been used.

Another source of error are the necessary simplifications and assumptions done during the modelling of the reactor. These include the exclusion of truncated conical extensions on the lateral surface of the conus, the omission of steel structures and material composition assumptions due to the lack of available data. The omission of the extensions from the core applies throughout the studies and is thus unlikely to affect the results. The steel structures do not have a significant effect on the operation and can be omitted without decreasing the accuracy of the model. Additionally, the lack of material data applies universally to the studies and thus should not affect the results.

Lastly, a source of error in the calculation can also be the parameters used in the simulation. These include the choices of libraries, the reactor physics codes used and the chosen number of neutron histories. The libraries used throughout the studies range from ENDF/B to JEF-2.2 and can have a noticeable effect on the result. The libraries used here, MCNP/B-VII, JEFF-3.1.1 and JENDL-4, differ from those of the prior studies, though the majority did use earlier versions of the MCNP library. The differences between the library versions, albeit probably minor, can have a slight effect on the result. In addition, the lack of some isotope data in the JENDL-4 library compared to the other two can be a source of error and thus cause the discrepancy between the results of different libraries.

A comparison between the ENDF/B-VII and JEFF-3.1 thermal scattering libraries, shown in table 7.3, displayed the effect using a different thermal scattering library has on the results. Both cases, the detailed and the simplified, were run using the ENDF/B-VII material library and the resulting subcriticality of the reactor with 16,890 using the JEFF-3.1 library was 2,234 pcm and 2,227 pcm for the detailed and simplified

cases respectively, compared to the ENDF/B-VII results of 2,266 pcm and 2,274 pcm. The amount of pebbles to reach criticality using the JEFF-3.1 was 17,917 with the detailed model and 17,940 with the simplified model. These results are 30–44 pebbles lower than those of the aforementioned ENDF/B-VII results. Thus it can be seen that the JEFF-3.1 thermal scattering library produces higher k_{eff} values compared to ENDF/B-VII.

Another comparison was performed using the DBRC option in Serpent in the detailed simulation of 16,890 pebbles using the ENDF/B-VII material library. The results from the table 7.4 show that the effect of enabling the option is only 4 pcm. Its effect is diminished due to the high enrichment of uranium-235 in the fuel.

The intrinsic differences within the different reactor physics codes, MCNP, VSOP, TRIPOLI and Serpent, can also be a major cause of differences in the results due to their different methods of calculation. The explicit modelling of the pebbles causes a small amount of carbon to overlap between adjacent pebbles. The delta-tracking method is not affected by this and it does not thus affect the calculations except through the loss of an insignificant amount of carbon. In addition, the lattice in MCNP used by the USA study did not allow for fuel and dummy pebbles of equal size. Thus they had to shrink the dummy pebbles while keeping its effect on the results minimal.

Finally, the amount of neutron histories also has a significant role on the error of the result. Given the nature of the Monte Carlo method, quadrupling the number of histories leads to the halving of the statistical error, increasing the number of neutron histories is an easy, if time intensive, way of reducing the error.

In this regard the prior studies used at most 5 million neutron histories in the calculations they based the interpolations on. This is lower than that of the Serpent model used in this thesis, where 600 and 1,200 million, varying on the simulation, neutron histories were generated to improve the precision. Thus the confidence intervals of the results of this study are over 10 times lower compared to that of the Iranian study, which had the highest history count of 5 million out of the prior studies.

8.4 Future developments

To investigate some of the potential sources of error it is advisable to simulate the reactor further in Serpent using regular lattices. This would produce a case closer to

those of the prior studies. Given the number of lattice types used in the prior studies, ranging from simple cubic to body centred cubic, multiple different types of regular lattices would be preferable.

The possible effects of localisation of moderator could be studied by generating multiple different beds of the same pebble amount. This would lower the effect the potential localisations have by increasing the sample size of the beds and thus reducing the likelihood of the moderator gathering in a given region.

Additionally, the effects of the temperature on the multiplication coefficient can be studied by changing the temperatures of the materials in Serpent to 293 K from the default 300 K. This would show the extent of the effect of the temperature difference between those used in the prior studies.

Chapter 9

Conclusion

The ability to model pebbles and fuel particles explicitly without the help of a lattice is important. It allows accurate modelling of pebble beds through the support of explicitly given, randomly located coordinates for pebbles and fuel particles. This is a significant improvement over the lattice-based approaches of other commonly used reactor physics codes since it removes that artificially introduced regularity in the core.

Through the addition of the elliptical surface the modelling capabilities of rectangular channels has improved in Serpent. The code of the surface could be modified to be applicable for a more general use, such as introducing options for the cylinder to be parallel to the x- or y- axis. However, already the ability of placing freely oriented rectangular surfaces parallel to the z-axis allows for a greater number of reactors to be modelled.

The required numbers of pebbles in the critical load gained from the simulations using JEFF-3.1 and ENDF/B-VII material libraries were, like most of the prior studies, higher than the empirical results. The Serpent models, however, resulted in even higher amounts of pebbles required to reach criticality. It is unknown how much of this difference is caused by the use of stochastic modelling for the pebbles and particles instead of lattices.

Monte Carlo method is a powerful tool in nuclear reactor modelling. With the increasing computational power available and constantly improving parallelisation in computing, many tasks previously impossible to simulate become feasible. Explicit modelling of spherical elements has not been possible in Monte Carlo due to its complexity, which has lead to time-consuming surface checks. However, with the use of delta-tracking the routines are made faster and the explicit models have become viable.

References

[1] A. Abedi, N. Vosoughi: *Neutronic simulation of a pebble bed reactor considering its double heterogeneous nature*. 2012. Nuclear Engineering and Design, Volume 253, pp. 277–284.

[2] A.F. Bielajew: *Fundamentals of the Monte Carlo method for neutral and charged particle transport*. 2001. [E-document]. From: http://www-personal.umich.edu/∼bielajew/MCBook/book.pdf, retrieved on 2014-10-14.

[3] J.J. Duderstadt, L.J. Hamilton: *Nuclear reactor analysis*. 1976. John Wiley & Sons.

[4] IAEA: *Current status and future development of modular high temperature gas cooled reactor technology*. 2001. [E-document]. From: http://www-pub.iaea.org/books/IAEABooks/6124/Current-Status-and-Future-Development-of-Modular-High-Temperature-Gas-Cooled-Reactor-Technology, retrieved on 2014-05-14.

[5] IAEA: *Evaluation of high temperature gas cooled reactor performance: Benchmark analysis related to initial testing of the HTTR and HTR-10*. 2003. [E-document]. From: http://www-pub.iaea.org/books/IAEABooks/6821/Evaluation-of-High-Temperature-Gas-Cooled-Reactor-Performance-Benchmark-Analysis-Related-to-Initial-Testing-of-the-HTTR-and-HTR-10, retrieved on 2014-05-13.

[6] IAEA: *Status Report 96 - High Temperature Gas Cooled Reactor - Pebble-Bed Module (HTR-PM)*. 2011. [E-document]. From: https://aris.iaea.org/sites/..\PDF\HTR-PM.pdf, retrieved on 2014-06-27.

[7] INSAG-10: *Defence in Depth in Nuclear Safety*. 1996. [E-document]. From: http://www-pub.iaea.org/MTCD/publications/PDF/Pub1013e_web.pdf, retrieved on 2014-12-04.

[8] IPCC: *Climate Change 2014: Synthesis Report*. 2014. [E-document]. From: http://www.ipcc.ch/report/ar5/syr/, retrieved on 2014-11-03.

[9] A.C. Kadak: *A future for nuclear energy: pebble bed reactors*. 2005. International Journal of Critical Infrastructures, Volume 1, Number 4, pp. 330–345.

[10] J.R. Lamarsh: *Introduction to Nuclear Reactor Theory*. 1966. Addison-Wesley Publishing Company Inc.

[11] J. Leppänen: *Development of a New Monte Carlo Reactor Physics Code*. 2007. [E-document]. From: http://montecarlo.vtt.fi/download/P640.pdf, retrieved on 2014-05-14.

[12] J. Leppänen: *Serpent - a Continuous-energy Monte Carlo Reactor Physics Burnup Calculation Code*. 2013. [E-document]. From: http://montecarlo.vtt.fi/download/Serpent_manual.pdf, retrieved on 2014-06-03.

[13] M.S.T. Price: *The Dragon Project origins, achievements and legacies*. 2012. Nuclear Engineering and Design, Volume 251, pp. 60–68.

[14] P. Reuss: *Neutron Physics*. EDP Sciences, 2008. ISBN 978-2-7598-0041-4.

[15] C.H. Rycroft et al.: *Granular flow in pebble bed reactors: dust generation and scaling*. 2012 International Congress on Advances in National Power Plants, Chicago, Illinois, 24th–28th June, 2012.

[16] H. Suikkanen: *Application and development of numerical methods for the modelling of innovative gas cooled fission reactors*. 2014. Doctoral dissertation. Lappeenranta University of Technology: Laboratory of Nuclear Engineering.

[17] VTT: *Serpent - A Monte Carlo Reactor Physics Burnup Calculation Code*. [Web page]. From: http://montecarlo.vtt.fi/, retrieved on 2014-07-29.

[18] WNA: *Nuclear Power in the World Today*. 2014. [E-document]. From: http://www.world-nuclear.org/info/Current-and-Future-Generation/Nuclear-Power-in-the-World-Today/, retrieved on 2014-10-21.

[19] WNA: *Nuclear Power Reactors*. 2014. [E-document]. From: http://www.world-nuclear.org/info/Nuclear-Fuel-Cycle/Power-Reactors/Nuclear-Power-Reactors/, retrieved 2014-12-03.

[20] WNA: *Thorium*. 2014. [E-document]. From: http://www.world-nuclear.org/info/current-and-future-generation/thorium/, retrieved on 2014-07-30.

[21] Z. Wu, D. Lin, D. Zhong: *The design features of the HTR-10*. 2002. Nuclear Engineering and Design, Volume 218, Issues 1–3, pp. 25–32.